

STRUCTURAL ENVIRONMENTS AROUND MOLYBDENUM IN SILICATE GLASSES AND MELTS. I. INFLUENCE OF COMPOSITION AND OXYGEN FUGACITY ON THE LOCAL STRUCTURE OF MOLYBDENUM

FRANÇOIS FARGES[§] AND RALF SIEWERT

Laboratoire de Minéralogie (USM 201), Muséum National d'Histoire Naturelle, CNRS UMR 7160, 61, rue Buffon, F-75005 Paris, France, and Department of Geological and Environmental Sciences, Stanford University, Stanford, California 94305-2115, USA

GORDON E. BROWN JR.

Department of Geological and Environmental Sciences, Stanford University, Stanford, California 94305-2115, and Stanford Synchrotron Radiation Laboratory, 2575 Sand Hill Road, MS 99, Menlo Park, California 94025, USA

ANNE GUESDON

Laboratoire CRISMAT – ENSICAEN, 6, Boulevard du Maréchal Juin, F-14050 Caen Cedex, France

GUILLAUME MORIN

Laboratoire de Minéralogie-Cristallographie, Universités de Paris 6, 7, IPGP and UMR CNRS 7590, 2, place Jussieu, F-75252 Paris Cedex 05, France

ABSTRACT

The coordination chemistry of molybdenum was investigated in nine series of synthetic silicate glasses, including sodium disilicate (NS2), sodium trisilicate (NS3), albite (Ab), anorthite (An), Ab₅₀An₅₀, Ab₃₀An₇₀, diopside (DI), rhyolite (RH), and basalt (BA), using electron paramagnetic resonance (EPR) and X-ray absorption fine structure (XAFS) spectroscopies. The Mo content of these glasses ranges from 300 ppm to 3 wt.%. On the basis of results derived from high-resolution X-ray absorption near-edge structure (XANES) spectroscopy, molybdenum is present primarily as molybdate moieties [Mo(VI)O₄²⁻] in most of the glass compositions prepared at *f*(O₂) values ranging from 1 atm to 10⁻¹² atm (temperatures ranging from 1100 to 1700°C, *i.e.*, from air to IW+4). Analysis of extended XAFS (EXAFS) spectra of these glasses indicates an average Mo–O distance of ~1.76(1) Å. No evidence for second-neighbor Si or Al around Mo was found in any of the glasses, confirming that molybdate moieties are not connected to the tetrahedral framework, in agreement with Pauling bond-valence predictions. The presence of molybdate moieties in regions of these glasses enriched in network modifiers helps explain why crystalline molybdates can nucleate easily in silicate glasses (and, by extension, in the corresponding melts). In the highly polymerized glass compositions (such as “Ab” or “RH”), Mo(VI)O₆⁶⁻ moieties also exist, but at minor levels (<20% of the total Mo). In glasses prepared at low *f*(O₂) (near IW), reduced species of Mo occur, such as molybdenyl [Mo(V) and Mo(IV)]. In glasses prepared at even lower *f*(O₂) (near IW+4), Mo is present as a metallic precipitate. The prevalence of molybdate moieties in silicate glasses until relatively low oxygen fugacities (IW) are achieved appears to be at variance with the fact that molybdenite, Mo(IV)S₂, is the dominant Mo-bearing mineral in the Earth’s crust. In a companion paper, we re-examine the speciation of molybdenum in more complex systems that are closer to geochemical reality, such as high-temperature melts, densified (high-pressure) glasses, and silicate glass compositions enriched in volatiles.

Keywords: molybdenum, glasses, melts, redox, XAFS spectroscopy, oxygen fugacity.

SOMMAIRE

La spéciation du Mo a été étudiée dans neuf séries de verres silicatés synthétiques: sodium di- et trisilicate (NS2, NS3), albite (Ab), anorthite (An), Ab₅₀An₅₀, Ab₃₀An₇₀, diopside (DI), rhyolite (RH) et basalte (BA), avec les spectroscopies RPE (paramagnétique électronique) et XAFS (d’absorption X). La teneur en Mo des verres varie entre 300 ppm et 3% (poids). Le XANES

[§] E-mail address: francoisfarges@gmail.com

haute résolution indique que Mo est présent sous forme d'unités molybdates $[\text{Mo(VI)O}_4^{2-}]$ dans la majorité des verres préparés à des $f(\text{O}_2)$ comprises entre 1 atm et 10^{-12} atm. L'EXAFS indique des distances Mo–O de $\sim 1.76(1)$ Å. Aucun second voisin Si ou Al n'a été détecté autour du Mo, confirmant que les unités molybdate sont déconnectées du réseau tétraédrique, en accord avec les prédictions de force de liaison de Pauling. Dans des compositions très polymérisées (comme "Ab" et "RH"), les entités Mo(VI)O_6^{6-} sont aussi détectées, mais à moins de 20% du molybdène total. La présence des unités molybdate dans ces verres explique pourquoi les molybdates cristallins nucléent facilement depuis ces compositions. Pour des verres préparés aux basses $f(\text{O}_2)$ (tampon IW), des états redox réduits du Mo sont détectés, comme Mo(V) et Mo(IV). Dans les verres synthétisés à encore plus basse $f(\text{O}_2)$ (IW–3), le molybdène précipite sous forme micro métallique. Cependant, la prévalence des unités molybdates dans des verres assez réduits (IW) semblent être en contradiction avec la géochimie du molybdène dans la croûte terrestre, où se forme plutôt de la molybdénite, Mo(IV)S_2 . Dans un travail connexe, nous examinons la spéciation du molybdène en conditions plus proches de la réalité géochimique, par exemple en conditions *in situ* (magmas à haute température et verres densifiés) et enrichis en fluides (H_2O , halogènes et soufre).

Mots-clés: molybdène, verre, magma, redox, spectroscopie XAFS, fugacité d'oxygène.

INTRODUCTION

Molybdenum is a 4d-transition element of major economic interest (Bookstrom 1999), because of its use in a number of high-technology alloys (accounting for 35% its production) as well as a catalyst and lubricant in the oil and gas industry (20% of the production). Economic deposits of molybdenum (primarily in the form of molybdenite, MoS_2) are limited to a few localities such as Climax (Colorado, USA), Luanchuan (Henan, China), and Chuquicamata (Atacama, Chile). Hence, owing to the strategic nature of molybdenum, there have been a number of studies of the genesis of molybdenum deposits in the Earth's upper crust (*e.g.*, Carten *et al.* 1993, Candela 1989, 1997, Hedenquist & Lowenstern 1994). Porphyry molybdenum deposits are intimately related to subvolcanic intrusions, and molybdenum also is produced as a by-product at many porphyry copper deposits. (*e.g.*, Keith & Shanker 1988, Candela & Bouton 1990, Webster 1999, Seedorff & Einaudi 2004). Subsequent hydrothermal fluids are considered to enrich these deposits in molybdenum (Isuk & Carman 1981, 1983, 1984, White *et al.* 1981, Tingle & Fenn 1984, Keppler & Wyllie 1991, Bai & Koster van Groos 1999, Schäfer *et al.* 1999). Hydroxy complexes of molybdenum are supposed to form in the aqueous or vapor phase as a result of a high fluid–melt partitioning (Isuk & Carman 1981, 1983, 1984, Candela & Holland 1984, Keppler & Wyllie 1991, Schäfer *et al.* 1999). Sulfur also strongly partitions into the aqueous or vapor phase (Isuk & Carman 1981, 1983, 1984), which depletes the melt in non-bridging oxygen atoms (as sulfate moieties above the NNO buffer), inducing then molybdenite precipitation according to Tingle & Fenn (1984). Geochemical investigations of molybdenum (a siderophile element with a strong chalcophile affinity) have focused on its thermodynamic behavior during magmatic crystallization, such as the partitioning of molybdenum among silicate melts, coexisting crystalline phases, and fluids under crustal conditions (*e.g.*, Candela & Holland 1984, 1986, Tacker & Candela 1987, Candela & Bouton 1990, Stemprok 1990, Keppler & Wyllie 1991, Candela 1997, Bai & Koster van Groos

1999, Schäfer *et al.* 1999, Kravchuk *et al.* 2000) as well as under conditions in the Earth's mantle, where metallic molybdenum is stable (*e.g.*, Inamura & Honda 1976, Palme & Rammensee 1981, Holzheid *et al.* 1994, Righter & Drake 1995, 1999, Walter & Thibault 1995, Hillgren *et al.* 1996), or in lunar regoliths, in which native molybdenum was also encountered (Bogatikov *et al.* 2001). If Mo(VI) and Mo(IV) are assumed to model the geochemistry of molybdenum in melts, Mo(V) needs to be investigated as well (Durasova *et al.* 1998), as its presence can blur the solubility data (this study), as already shown in oxide glasses for nuclear wastes.

The behavior of molybdenum in aluminosilicate and borosilicate glasses is of interest because of its nucleating properties, especially in glass compositions selected for nuclear waste containment (Camara *et al.* 1979, Horneber *et al.* 1982, Petit-Maire 1988, Faure 1998, Farges *et al.* 1990, Sawaguchi *et al.* 1996, Calas *et al.* 2003, Short *et al.* 2005). The decay of high-activity actinides such as ^{235}U , Np, Pu, Am in these silicate glasses produces a significant amount of molybdenum (commonly over 1 wt.%), which could affect the long-term durability of its host matrix (*e.g.*, Faure 1998). For instance, most of the world's supply of ^{99}Mo , which decays into ^{99}Tc (an important isotope used in medical diagnostics), is produced by the fission of ^{235}U in highly enriched uranium fuels. Finally, the incorporation of molybdenum in silicate glasses is a potential process for immobilizing bioavailable molybdenum in polluted sediments, soils, and chemical and medical wastes (*e.g.*, Helz *et al.* 1996, Erickson & Heltz 2000, Adelson *et al.* 2001).

Little direct and detailed information is available on the coordination chemistry of molybdenum in (alumino-) silicate glasses (*e.g.*, Calas 1981, Farges *et al.* 1990, Siewert *et al.* 1997a, 1998, Durasova *et al.* 1998, 1999) or melts (Siewert *et al.* 1997b) of geological interest, in contrast to solubility information (Holzheid *et al.* 1994, Walter & Thibault 1995, O'Neill & Eggins 2002). However, all solubility studies are based on indirect measurements and only Mo(IV) and Mo(VI) have been considered. Neither the possible presence of Mo(V) nor Mo(III) was taken into account, although it has been

reported previously (Camara *et al.* 1979, Horneber *et al.* 1982, Petit-Maire 1988, Farges *et al.* 1990, Siewert *et al.* 1998, Short *et al.* 2005). There are a number of spectroscopic methods capable of providing this information, including X-ray absorption fine structure (XAFS), X-ray photoemission spectroscopy (XPS), vibrational (infrared/Raman scattering), electron paramagnetic resonance (EPR), optical (UV–visible–NIR, including magnetic circular dichroism), and laser-induced fluorescence spectroscopies. However, the last three methods are not sensitive to some molybdenum oxidation states. EPR is sensitive to Mo(V) and Mo(III) only, whereas UV–visible–NIR is not sensitive to Mo(V, IV, III) [the brownish color related to Mo(V) is difficult to quantify]. Only XAFS spectroscopy is sensitive to all oxidation states of molybdenum at trace levels (as low as 100 ppm), and has become the method of choice for determining the structural environment of trace elements in silicate glasses and melts to a radial distance of a few Å (*e.g.*, Brown *et al.* 1988, 1995, Henderson *et al.* 1995), including their oxidation states.

In this study and a companion study (Farges *et al.* 2006), we present a systematic examination of the coordination chemistry of molybdenum in selected silicate glasses and silicate melts using XAFS and EPR spectroscopies. The present study focuses on the influence of composition (including the ratio of non-bridging oxygen atoms to tetrahedra, NBO/T) and oxygen fugacity on the local environment of molybdenum in quenched glasses. In the companion paper, we examine the effect of pressure and temperature (*in situ*) as well as the presence of “volatiles” (H₂O, halogens and sulfur) on the local structural environment of molybdenum in selected silicate glasses and melts. Included in the present study is a series of molybdenum-bearing crystalline oxide model compounds of known structure. Detailed analysis of the XAFS spectra of these compounds provides a more quantitative basis for interpreting the glass/melt XAFS spectra. Earlier papers in this series on incompatible, high-valence trace elements in silicate melts and glasses focused on Zr(IV) (Farges *et al.* 1991) and U(IV,V,VI) (Farges *et al.* 1992).

EXPERIMENTAL

Model compounds

A variety of Mo-containing model compounds were synthesized or obtained from mineral collections to help understand the spectral features of molybdenum and their variations with the redox state of molybdenum. The MoO₃ compound studied is the reagent-grade (Merck) orthorhombic modification (molybdite; Kihlborg 1963). Several synthetic molybdate-bearing compounds were studied, including reagent-grade lithium, sodium, and ammonium molybdates. Natural molybdates include wulfenite (PbMoO₄, from Chihuahua, Mexico; Leciejewicz 1965) and powellite (CaMoO₄, from Poona, India;

Aleksandrov *et al.* 1967). Molybdenite (MoS₂, from Pontiac, Quebec) was ground slowly in acetone and dispersed using ultrasonics to avoid preferred orientations owing to its very low hardness (1 on Mohs scale). These minerals are from the Stanford University mineral collection. Synthetic Y₂TiMoO₈ was prepared using a high-temperature solid-state reaction of TiO₂, Y₂O₃, and MoO₃ (Blasse 1968). Ammonium molybdate [(NH₄)₂Mo(VI)₂O₇] (poorly X-ray-diffracting), Mo(V) isopropoxyl [Mo(OC₃H₇)₅, liquid], and MoO₂ are reagent-grade chemicals from Merck Inc. (Bendor & Shimony 1974, Averbuch-Pouchot 1988). Lithium, and sodium molybdates (Li₂MoO₄, Na₂MoO₄•2H₂O) are reagent-grade chemicals from Prolabo SA (Tretyak *et al.* 1974, Matsumoto *et al.* 1975). Finally, a selection of molybdenum phosphates were synthesized at the ISMRA (Caen, France) with molybdenum present in various redox states: NaMo(III)P₂O₇ (Leclaire *et al.* 1988), KMo(IV)P₃O₁₂ (Leclaire & Raveau 1988), Cs₆Mo(IV)₇PO₁₃•H₂O (Guesdon *et al.* 1994), β-K₂Mo(V)₂P₂O₁₁ (Guesdon *et al.* 1995), AgMo(V,VI)₃P₂O₁₄ (Savary *et al.* 1997).

Synthesis of glass samples

Glasses of sodium disilicate and trisilicate compositions (labeled NS2 and NS3, respectively) were synthesized from dehydrated, high-purity Na₂CO₃ and silica glass (Herasil 1, Heraeus Quarzschmelze, Hanau). Glasses having the composition of albite (Ab), Ab₅₀An₅₀ and Ab₃₀An₇₀ (An: anorthite) were prepared from high-purity oxides by Schott Glaswerke, GmbH. Glasses of diopside, rhyolitic, and basaltic composition were synthesized from high-purity grade oxides by Prolabo SA. These samples were ground in an agate mortar to a grain size <200 μm and were mechanically mixed with either 300, 1000, 2000, 10000 or 30000 ppm molybdenum, which was added in form of high-purity MoO₃ (one glass of Ab composition was synthesized with MoO₂ to check for equilibrium kinetics; see below). Batches of 700 mg of each mixture were melted in a vertical tube gas-mixing furnace using Pt crucibles 14 mm in diameter. In order to reach equilibrium more quickly, the diffusion path-length of oxygen in the melt was minimized by using large platinum plates (instead of Pt crucibles) to equilibrate the glasses rich in the albite component, leading to approximately 2-mm-thick sheets of glass after quenching. The melts were equilibrated either in air or under an H₂–CO₂–Ar–N₂ atmosphere (Table 1) for 6 hours at 1100°C (NS2 and NS3 compositions), at 1300°C (albite composition), at 1500°C (diopside, basalt and rhyolite compositions) and at 1650°C (An₁₀₀, Ab₅₀An₅₀ and Ab₃₀An₇₀ compositions). These conditions of oxygen fugacity range from air to ~4 log units below the iron–wüstite (IW) buffer. A PtRh₆/PtRh₃₀ thermocouple and a CaO–Y₂O₃-stabilized solid ZrO₂ electrolytic oxygen sensor were used to measure temperature and oxygen fugacity, *f*(O₂),

respectively, during the experiments. Oxygen fugacity was checked against the IW buffer, and its accuracy was found to be ± 0.3 log units on average. The melts were quenched by externally cooling the Pt crucible with cold water. The color of the quenched glasses ranges from transparent (95% of the glasses) to light brownish [glasses prepared at $f(\text{O}_2)$ of 10^{-10} to 10^{-12} atm at 1100–1300°C, equivalent to MW–IW buffers] to black (IW–4) and was, in each case, homogeneous to the eye. The NS2 and NS3 glasses were free of bubbles, whereas the glasses of albite composition contained a large number of small bubbles. Because the glasses were ground again before XAFS measurements, the bubbles in the glasses had no measurable effect on data collection.

Checking the quality of the glass

Molybdenum is known to dissolve in large quantities (>5 wt.%) as MoO_3 in silicate glasses (see Stemprok & Voldan 1974). However, in order to check if time and temperature were sufficient to reach redox equilibrium, two glasses of albite composition were synthesized simultaneously with molybdenum added as either Mo(IV)O_2 or Mo(VI)O_3 . This synthesis run was performed in air, in which case Mo(VI) is predicted to be stable (as verified by XAFS) and is less able to diffuse owing to its higher nominal charge. No differences were observed in the molybdenum K -edge XAFS spectra for the two glasses of Ab composition. In addition, no Mo–Mo pair correlations (like in crystalline MoO_3 or MoO_2) were observed in any of the glass samples studied, suggesting that molybdenum is dissolved at the ångström scale in our samples. In the most reduced black glasses, no evidence for crystalline domains containing metallic molybdenum was observed by X-ray diffraction, suggesting that metallic molybdenum precipitated. In addition, because the melts of albite composition are the most viscous compositions investigated (resulting in the highest diffusion-time for oxygen among the investigated compositions of melt), redox equilibrium is assumed to have been reached for the other melts, given the fact that various starting assemblages resulted in comparable final glasses (at least in terms of their Mo local structure). A summary of all synthesis conditions is given in Table 1. Results of chemical analyses (electron-microprobe data) for selected glasses (Table 2) are within 1% of their nominal compositions.

The collection of XAFS data

XAFS spectra of glasses and crystalline model compounds were collected at the Stanford Synchrotron Radiation Laboratory (SSRL, Stanford, USA) using beamlines 4–1 and 4–3. The storage ring was operating at 3 GeV and 50–100 mA electron current. XAFS spectra were collected at the molybdenum K -edge

(20,000 eV). A Si (220) double-crystal monochromator (detuned 25% to eliminate most of the higher-energy harmonics) was used, providing an energy resolution of ~ 5 eV at the molybdenum K edge. X-ray absorption near-edge structure (XANES) spectra were measured under conditions of relatively high resolution [0.3 mm slits after the Si(220) monochromator], whereas EXAFS data were collected at lower resolution (*i.e.*, with 2.0 and 1.0 mm slits before and after the monochromator, respectively). The energy calibration of the monochromator was repeatedly checked against the absorption spectrum of metallic molybdenum or sodium molybdate dihydrate in the transmission mode, leading to an accuracy of ~ 0.2 eV for the energy of the measured spectra. XAFS spectra (either XANES or EXAFS) for diluted glasses were collected in the fluorescence mode, using a Stern–Heald-type detector (Lytle *et al.* 1984), filled

TABLE 1. CONDITIONS OF SYNTHESIS OF THE GLASS SAMPLES INVESTIGATED

Run No.	sample	initial Mo (ppm)	T (°C)	atmosphere	log $f(\text{O}_2)$	duration (hours)
1a	NS2	1000	1104	H ₂ -CO ₂ -N ₂	-7.9	6
2a	NS2	1000	1104	H ₂ -CO ₂ -N ₂	-10.5	6
4a	NS2	1000	1104	H ₂ -CO ₂ -N ₂	-11.5	5
5a	NS2	1000	1104	H ₂ -CO ₂ -N ₂	-14.4	6
6a	NS2	1000	1104	air	-0.7	6
7a	NS2	1000	1104	H ₂ -CO ₂ -Ar	-2.1	6
8a	NS2	1000	1104	H ₂ -CO ₂ -Ar	-4.7	6
9a	NS2	1000	1104	H ₂ -CO ₂ -Ar	-5.6	6
10a	NS2	1000	1104	H ₂ -CO ₂ -Ar	-3.5	6
11a	NS2	1000	1104	H ₂ -Ar	-16.2	6
1b	NS3	2000	1104	H ₂ -CO ₂ -N ₂	-7.9	6
2b	NS3 (+Fe)	2000	1104	H ₂ -CO ₂ -N ₂	-10.3	6
3b	NS3 (+Fe)	2000	1104	H ₂ -CO ₂ -N ₂	-8.0	6
4b	NS3	2000	1104	H ₂ -CO ₂ -N ₂	-11.9	5
5b	NS3 (+Fe)	2000	1104	H ₂ -CO ₂ -N ₂	-14.4	6
6b	NS3	2000	1104	air	-0.7	6
7b	NS3	2000	1104	H ₂ -CO ₂ -Ar	-2.1	6
8b	NS3	2000	1104	H ₂ -CO ₂ -Ar	-4.7	6
9b	NS3	2000	1104	H ₂ -CO ₂ -Ar	-5.9	6
10b	NS3	2000	1104	H ₂ -CO ₂ -Ar	-3.5	6
11b	NS3	2000	1104	H ₂ -Ar	-16.5	6
12	NS3	2000	1100	H ₂ -CO ₂ -Ar	-13.2	6
13	NS3 (+Fe)	2000	1100	H ₂ -CO ₂ -Ar	-12.0	6
14	NS3	2000	1100	H ₂ -CO ₂ -Ar	-14.0	6
14b	NS3	2000	1100	H ₂ -CO ₂ -Ar	-15.1	6
14c	NS3	2000	1110	H ₂ -CO ₂ -Ar	-12.5	6
14d	NS3	2000	1110	H ₂ -CO ₂ -Ar	-10.5	6
14	Ab	2000	1300	H ₂ -CO ₂ -Ar	-8.9	6
15	Ab	2000	1300	H ₂ -CO ₂ -Ar	-10.2	6
16	Ab	2000	1300	H ₂ -CO ₂ -Ar	-11.0	6
17	Ab	2000	1300	H ₂ -CO ₂ -Ar	-12.0	6
18	Ab	2000	1300	air	-0.7	6
19	Ab ^a	2000	1300	air	-0.7	6
20	Ab ₅₀ Am ₅₀	2000	1650	air	-0.7	6
21	Ab ₃₀ Am ₇₀	2000	1650	air	-0.7	6
22a	Am ₁₀₀	2000	1650	H ₂ -CO ₂ -Ar	-8.0	5
22b	Am ₁₀₀	2000	1650	air	-0.7	6
23a	Di	30000	1500	H ₂ -CO ₂ -Ar	-7.0	3
23b	Di	30000	1500	H ₂ -CO ₂ -Ar	-8.9	3
23c	Di	30000	1500	H ₂ -CO ₂ -Ar	-10.0	3
23	rhyolite	300	1500	air	-0.7	10
25	rhyolite	1000	1500	air	-0.7	10
25b	rhyolite	20000	1500	air	-0.7	10
26	basalt	20000	1600	H ₂ -CO ₂ -Ar	-8.0	3

^a Mo added as MoO_2 (MoO_3 in all other glasses).

with argon. A six-absorption-length Zr foil was used to filter elastic scattering from the molybdenum $K\alpha$ fluorescence signal). XAFS spectra for model compounds were collected in the transmission mode to minimize self-absorption effects. Intensities of incident and transmitted beam were monitored using ionization chambers filled with nitrogen and argon gas, respectively.

The analysis of XAFS data

The molybdenum K -edge XANES spectra were normalized using conventional methods, by fitting a Victoreen function before the edge and an arctangent function after the edge. The XAFS data-analysis package, version 2.6 (Winterer 1997) was used for this step and subsequent steps in the XANES analysis and for fitting the EXAFS data. The pre-edge features (located near 20,000 eV) were normalized by fitting the edge jump as a background signal (using a combination of pseudo-Voigt functions). The normalized pre-edge feature was then modeled using a single pseudo-Voigt function (which converged to a highly

Gaussian shape) to derive its centroid position, normalized height and full width at half maximum (FWHM). The EXAFS spectra were normalized in absorbance using Victoreen (before the edge) and a combination of cubic spline functions (after the edge). Energies were recalculated into k space, where k is the photoelectron wavenumber (Teo 1986). In order to better visualize the various contributions to the k^3 -weighted EXAFS, the latter were Fourier-transformed over the k -window range 1.4–13.5 \AA^{-1} using a Kaiser–Bessel apodization function. However, we modeled the normalized k^3 -weighted EXAFS oscillations (*i.e.*, not FT-filtered), assuming a curved-wave anharmonic formalism (Rehr *et al.* 1986, Farges *et al.* 1996) and back-scattering amplitude and phase-shift functions extracted from the $\text{Na}_2\text{MoO}_4 \cdot 2\text{H}_2\text{O}$ model compound (Matsumoto *et al.* 1975). *Ab initio* molybdenum K -edge XANES and EXAFS calculations were undertaken using FEFF versions 8.28 and 7.02, respectively (Ankudinov *et al.* 1998, Rehr *et al.* 1992).

EPR spectroscopy

Electron paramagnetic resonance (EPR) spectroscopy (or ESR, electron-spin resonance) is a powerful method in the study of atoms with unpaired electrons (see Calas 1988, Morin & Bonnin 1999 for geological applications of EPR spectroscopy). Pentavalent and trivalent molybdenum both have one unpaired $4d$ electron, and EPR can provide information on the local symmetry around these two ions, as well as on their ligands bound to each of these paramagnetic centers. In addition, EPR can be used to measure the absolute concentration of Mo(V), the only EPR-active oxidation state of molybdenum. EPR spectra were collected at 9.42 GHz (X band) hyperfrequency using a ESP300E Bruker spectrometer (Laboratoire de Minéralogie–Cristallographie, Paris) operating at room temperature in the range 40–6000 G. We used a 100 kHz modulation frequency, a 5.0 G modulation amplitude, 100 mW microwave power, a receiver gain of 8000, and a time constant of 0.163 s to obtain the best signal-to-noise ratio for the glass samples investigated in this study. The EPR spectra are described by their effective g values, where g is the EPR spectroscopic factor defined by the relation $h\nu = g\beta H$, where h is Planck's constant, ν is the resonance frequency, β is the Bohr magneton, and H is the field strength at which resonance occurs. The g values were calibrated by comparison with a standard (1,1-diphenyl-2-picryl-hydrazyl, DPPH, $g = 2.00037 \pm 0.0002$), with an instrumental error of ± 0.001 . The EPR signal for Mo(V) and Mo(III) appears near g values of 1.94 and 5.19, respectively (Durasova *et al.* 1998). Glass powders (same mass for each sample: 70 mg) were placed in calibrated silica tubes (suprasil grade). A series of four silicate glasses approximately of $\text{CaNaAlSi}_5\text{O}_{18}$ composition, CNS4 (or calcium–sodium tetrasilicate) doped with 10, 100, 1000 ppm and 1

TABLE 2. COMPOSITIONS OF SELECTED GLASSES¹

sample	SiO ₂	Al ₂ O ₃	CaO	MgO	Na ₂ O	K ₂ O	MoO ₃	Σ	NBO/T
Ab air	69.1	19.1			11.7		0.16	100.2	~0.0
Ab -8.9	70.2	18.6			12.0		0.18	101.0	
Ab -10.3	69.0	18.9			12.1		0.27	100.3	
Ab -11.0	69.9	18.9			12.2		0.15	101.2	
Ab -12.2	69.3	19.0			12.0		0.21	100.5	
Ab ₅₀ An ₅₀	54.8	28.6	10.2		5.9		0.27	99.8	~0.0
Ab ₅₀ An ₇₀	50.4	31.6	14.0		3.7		0.15	99.9	
NS2 air	68.9				30.5		0.16	99.6	~1.0
NS2 -3.5	70.6				30.5		0.29	101.4	
NS2 -5.3	70.9				28.5		0.25	99.7	
NS2 -8.0	68.5				30.5		0.05	99.1	
NS2 -10.5	70.9				28.4		0.13	99.4	
NS2 -11.9	69.6				30.2		0.13	99.9	
NS2 -14.4	70.0				29.8		0.18	100.0	
NS3 air	76.0				22.7		0.30	99.0	~0.7
NS3 -3.5	73.9				23.8		0.35	98.1	
NS3 -5.3	74.5				24.3		0.30	99.1	
NS3 -7.9	74.1				24.5		0.30	98.9	
NS3 -10.5	76.3				22.2		0.19	98.7	
NS3 -11.9	76.1				22.4		0.13	98.6	
NS3 -14.4	76.4				22.4		0.11	98.9	
Di 3% (10 ²⁵)	53.1		24.7	17.2			4.2	98.9	~1.0
Di 3% (10 ²⁶)	53.7		25.2	16.8			3.9	99.6	
An	42.4	34.7	19.5				3.3	99.9	~0.0
Basalt (1%) ²	46.0	15.2	9.8	7.0	4.4	2.8	1.0	100.2	~0.7
Rhyolite (2%) ³	69.8	14.2	1.2	0.2	2.7	4.8	2.4	97.1	~0.1
Rhyolite (0.1%) ⁴	73.9	12.8	1.1	0.3	2.7	4.6	0.2	98.2	~0.0
average error	1.0	0.5		0.4	0.7		0.03		

¹ Average compositions resulting from 4–10 individual analyses for each glass. Results of electron-microprobe analyses, expressed in wt.%. Experimental conditions: 15 kV, 5 mA, spot size: 8 μm , 10 seconds counting time per element. ² Includes 1.9 wt.% TiO₂ and 12.1 wt.% FeO. ³ Includes 0.1 wt.% TiO₂ and 1.7 wt.% FeO. ⁴ Includes 0.2 wt.% TiO₂ and 2.4 wt.% FeO.

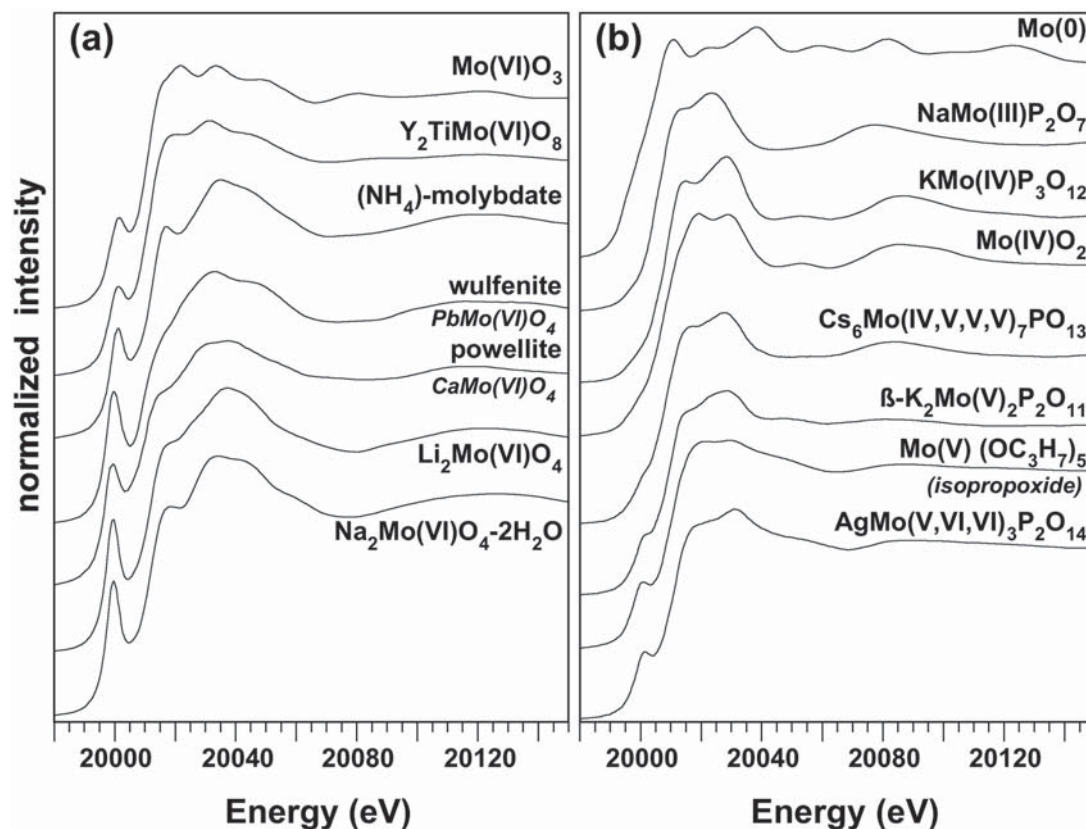


FIG. 1. High-resolution Mo K -edge XANES spectra for selected model compounds with Mo(VI) (left) and MoO, Mo(III), Mo(IV) and Mo(V) (right).

wt.% Cu^{2+} (as CuO) were used to calibrate the EPR spectrometer in order to derive the spin concentration in the unknown Mo(V)-bearing glasses. We did not use standard Mo(V) model compounds, as they are commonly organic dimers (Guesdon *et al.* 1995) that are not likely to form at trace levels in silicate glasses, owing to their low contents of Mo and their organic nature. The EPR spectra were integrated to derive the sample's absorbance; the integrated area gives the spin concentration of the sample.

RESULTS ON MODEL COMPOUNDS

Pre-edge features

Figure 1 shows molybdenum K -edge spectra collected for 15 model compounds, in which molybdenum (0, III, IV, V or VI) is located in 4-, 5-, 6-, and 8-coordinated sites. Where the oxidation state of molybdenum is hexavalent, an intense pre-edge is observed in the molybdenum K -edge spectrum, especially in a local

structural environment with T_d symmetry (*i.e.*, with no center of symmetry). These pre-edges are located near 20,000(5) eV, *i.e.*, 20–30 eV before the main-edge crest (Fig. 1a). A pre-edge is also observed in the XANES spectra for Mo(V)- and Mo(IV)-containing model compounds (Fig. 1b), but the intrinsic resolution of the experiments (4.5 eV core-hole-lifetime broadening and 1.5 eV experimental broadening; see Krause & Oliver 1979) is not high enough to clearly resolve this feature (only a shoulder is observed in the edge jump). By analogy to 3d transition elements (*e.g.*, Calas & Petiau 1983, Dräger *et al.* 1988, Farges *et al.* 1997, 2001, Heumann *et al.* 1997, Wilke *et al.* 2001), these features are mainly related to dipolar $1s \rightarrow 4d$ electronic transitions for molybdenum. In addition, quadrupolar $1s \rightarrow 4d$ transitions and dipolar $1s \rightarrow 2p$ transitions (to O first neighbors or molybdenum second neighbors, where present; see Dräger *et al.* 1988, Heumann *et al.* 1997) are most likely present, but are less intense (Brouder 1990). The intensity of this transition increases (see Fig. 1b) as the 4d states become emptier, *i.e.*, with

increasing oxidation state of the molybdenum (*i.e.*, from MoO₂ to MoO₃).

FEFF calculations

In order to verify these trends, *ab initio* molybdenum *K*-edge XANES calculations were performed (Fig. 2) using the FEFF 8.28 package (Ankudinov *et al.* 1998) on various clusters around molybdenum, extracted from various model compounds (default settings were used). Examination of Figure 2 confirms that the intense pre-edge feature observed in *K*-edge XANES spectra of molybdate-bearing compounds is related to the Mo(VI)O₄ units [*i.e.*, tetrahedrally coordinated Mo(VI) moieties], in agreement with Evans & Mosselmans (1991) and Kuzmin & Grisenti (1994). Where 6-coordinated, Mo(VI) shows no well-defined pre-edge feature, but has an additional shoulder (possibly a 1s → 5*d* transition). Therefore, the presence of this pre-edge

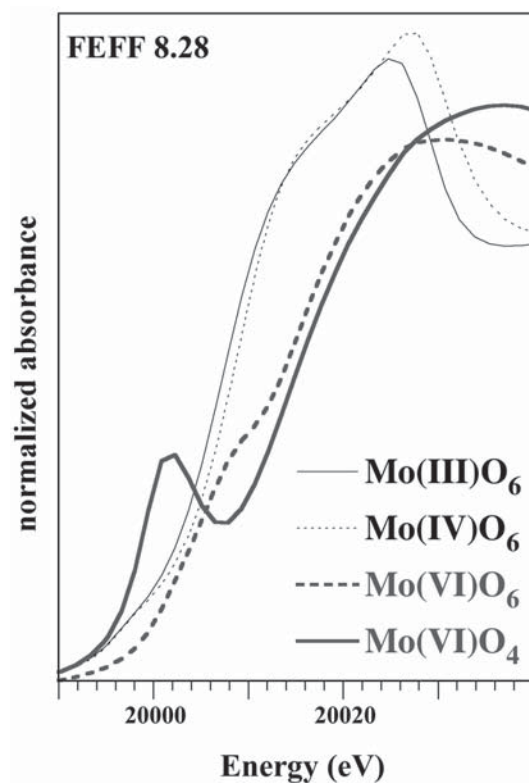


FIG. 2. Calculated *ab initio* XANES spectra at the Mo *K*-edge in selected clusters, showing that the intense pre-edge feature for Mo(VI) arise from molybdate moieties [Mo(VI)O₄ cluster], whereas that for a Mo(IV)O₆ cluster is much lower in height. The pre-edge for Mo(IV) and Mo(III) is weak, but shows the shift of the edge position with the redox state.

feature is a clear spectroscopic signature of Mo(VI)O₄ moieties (molybdates). On the basis of these calculations, experimental XANES spectra can be modeled assuming two pseudo-Voigt functions for the 1s → 4*d* and 1s → 5*d* pre-edge features and an arctangent function for the atomic absorption, μ_0 (Fig. 3a).

Pre-edges for mixtures of Mo environments

The pre-edge feature of Mo(VI) in octahedral symmetry [*e.g.*, ¹⁶Mo(VI)O₃] occurs at a higher energy than Mo(IV) in tetrahedral symmetry [*e.g.*, ¹⁴Mo(VI)O₄]. In addition, the normalized height of the pre-edge feature decreases significantly as a result of the increase in centrosymmetry, which makes dipolar transitions less likely. The same trends were observed for Ti(IV); see Farges *et al.* (1997) for details. As for Ti(IV), a non-linear variation between the pre-edge and the pre-edge normalized energy-positions is observed for mechanical mixtures of ¹⁴Mo(VI) (as NaMoO₄•2H₂O) and ¹⁶Mo(VI) (as MoO₃; Fig. 3b). For mixtures of ¹⁴Mo(VI) with compounds with lower oxidation states of molybdenum, pre-edge information is more difficult to measure because of the low pre-edge height for these mixtures (lower oxidation states of molybdenum have fewer unfilled 4*d* levels, making electronic transitions from 1s levels less probable or detectable). For mixtures of compounds containing ¹⁴Mo(VI) and ¹⁶Mo(IV), the pre-edge information for the NaMoO₄•2H₂O and MoO₂ was analyzed (see Fig. 3b). This information will be used to further constrain changes in redox and coordination of molybdenum with oxygen fugacity and melt composition.

Edge position

As the oxidation state of molybdenum decreases from VI to IV, and then to III, the pre-edge feature of molybdenum becomes too weak to be observed (Fig. 1b), in agreement with *ab initio* XANES calculations (Fig. 2). In parallel, the edge position is shifted toward lower energies (by ~10 eV) (Fig. 4a, Table 3), in agreement with previous studies (Savary *et al.* 1997) and *ab initio* XANES calculations (Fig. 2). Therefore, determination of the oxidation state of molybdenum must be performed near 20020 eV to minimize interferences from the pre-edge feature, where significant (Fig. 3a). In this case, we chose an edge position defined as the energy where the edge jump equals 1 (Fig. 4a). The edge position for the model compounds studied shows a quasi-linear variation with the average state of oxidation of molybdenum (Fig. 4b).

EXAFS and FT

Figure 5 shows the *k*³-weighted, normalized EXAFS spectra for selected model compounds (Fig. 5a) and their corresponding Fourier transforms (FT) (Fig. 5b).

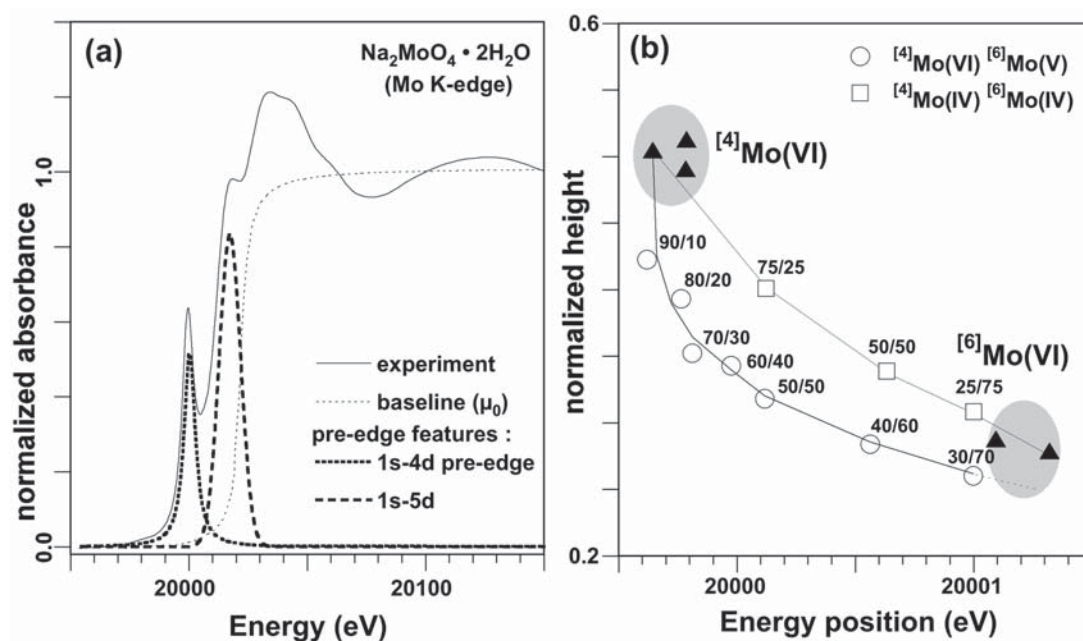


FIG. 3. Pre-edge analysis at the Mo K-edge. (a) Deconvolution of the XANES region, showing the need to consider two electronic transitions ($1s$ to $4d$, and $5d$ levels, respectively) to extract reliable information for the first pre-edge feature. (b) Variation in the pre-edge information (position *versus* normalized height) for model compounds of Mo and their mechanical mixtures (experimental information) showing a pre-edge feature [4-, and 6-coordinated Mo(VI) and Mo(IV), as $\text{NaMoO}_4 \cdot 2\text{H}_2\text{O}$, MoO_3 and MoO_2 , respectively]. Solid triangles corresponds to the pre-edge information for model compounds of Mo(VI) and Mo(IV) of that study. The gray areas enclose the pre-edge information that is typical of molybdate [*e.g.*, Mo(VI)O_4^{2-}], and Mo(IV)O_6^{8-} moieties.

TABLE 3. INFORMATION ON OXIDATION STATE OF Mo FOR MODEL COMPOUNDS AND Mo-BEARING SILICATE GLASSES

Model compound	Energy at $\mu=1.0$	Average Mo-redox	Glass	Energy at $\mu=1.0$	Average Mo-redox
$\text{Na}_2\text{MoO}_4 \cdot 2\text{H}_2\text{O}$	20014.7	6.0	NS3 air	20015.0	6.0
Li_2MoO_4	20014.6	6.0	NS3 -2.6	20015.0	6.0
powellite	20013.5	6.0	NS3 -3.5	20014.5	6.0
wulfenite	20015.0	6.0	NS3 -5.4	20014.5	6.0
$(\text{NH}_4)_2\text{Mo}_2\text{O}_7$	20013.3	6.0	NS3 -5.9	20015.0	6.0
YTiMoO_4	20014.2	6.0	NS3 -8.0	20014.5	6.0
MoO_3	20013.1	6.0	NS3 -10.5	20014.5	6.0
$\text{AgMo}_2\text{P}_2\text{O}_{14}$	20012.9	5.7	NS3 -10.3	20015.0	6.0
$\text{Mo}(\text{OC}_2\text{H}_5)_2$	20012.4	5.0	NS3 -11.9	20014.5	6.0
$\beta\text{-K}_2\text{Mo}_2\text{O}_7 \cdot \text{P}_2\text{O}_7$	20011.5	5.0	NS3 -12.5	20013.9	6.0
$\text{C}_8\text{H}_8\text{Mo}_2\text{O}_{29}(\text{PO}_4)$	20010.8	4.7	NS3 -13.2	20012.9	5.5
MoO_2	20010.5	4.0	NS3 -14.0	20011.9	5.0
$\text{KM}_2\text{P}_2\text{O}_{12}$	20010.1	4.0	NS3 -14.4	20012.0	4.9
NaMoP_2O_7	20008.0	3.0	NS3 -16.5	20007.6	2.4
Mo^0 metal foil	20004.3	0.0	NS2 air	20015.5	6.0
			NS2 -2.1	20016.0	6.0
Ab air (Mo as MoO_3)	20016.0	6.0	NS2 -3.5	20015.5	6.0
Ab air (Mo as MoO_2)	20016.5	6.0	NS2 -3.9	20015.5	6.0
Ab -8.9	20016.0	6.0	NS2 -5.6	20016.0	6.0
Ab -10.2	20015.5	6.0	NS2 -7.9	20015.5	6.0
Ab -11.0	20014.5	6.0	NS2 -10.5	20016.0	6.0
Ab -12.2	20011.5	4.8	NS2 -11.5	20017.5	6.0
			NS2 -14.4	20016.5	6.0
			NS2 -16.2	20010.0	3.9
average error	0.1	0.2		0.1	0.2

Major differences in the EXAFS spectra are consistent with large differences in the speciation of molybdenum in these model compounds. The most noteworthy models for this study are metallic molybdenum (with a strong Mo–Mo pair correlation near 2.8 Å in the FT, uncorrected for phase shifts), molybdenite (with S ligands, located at a much higher distance in the FT as compared to oxygen ligands), various alkali and alkaline earth molybdates, and molybdenum(V) isopropoxyl. Pentavalent-molybdenum-bearing compounds are characterized by the presence of molybdenyl complexes. These moieties are composed of two well-separated shells of oxygen atoms with a short covalent Mo=O bond (near 1.7 Å) and four to five more distant Mo–O bonds ranging from 1.9 to 2.2 Å (as in $\beta\text{-K}_2\text{Mo}_2\text{O}_7 \cdot \text{P}_2\text{O}_7$; Guesdon *et al.* 1995; see also McMaster *et al.* 2001). These moieties are also known in aperiodic compounds such as glasses, as confirmed by EPR studies of several Mo(V)-bearing glasses (see, *e.g.*, Bobkova *et al.* 1989, Cozar *et al.* 1993, Boudlich *et al.* 1998). Results of EXAFS fits for the Mo–O pair in powellite, molybdate, and MoO_2 , presented in Table 4, show excellent agreement with results of crystal-structure refinements. On

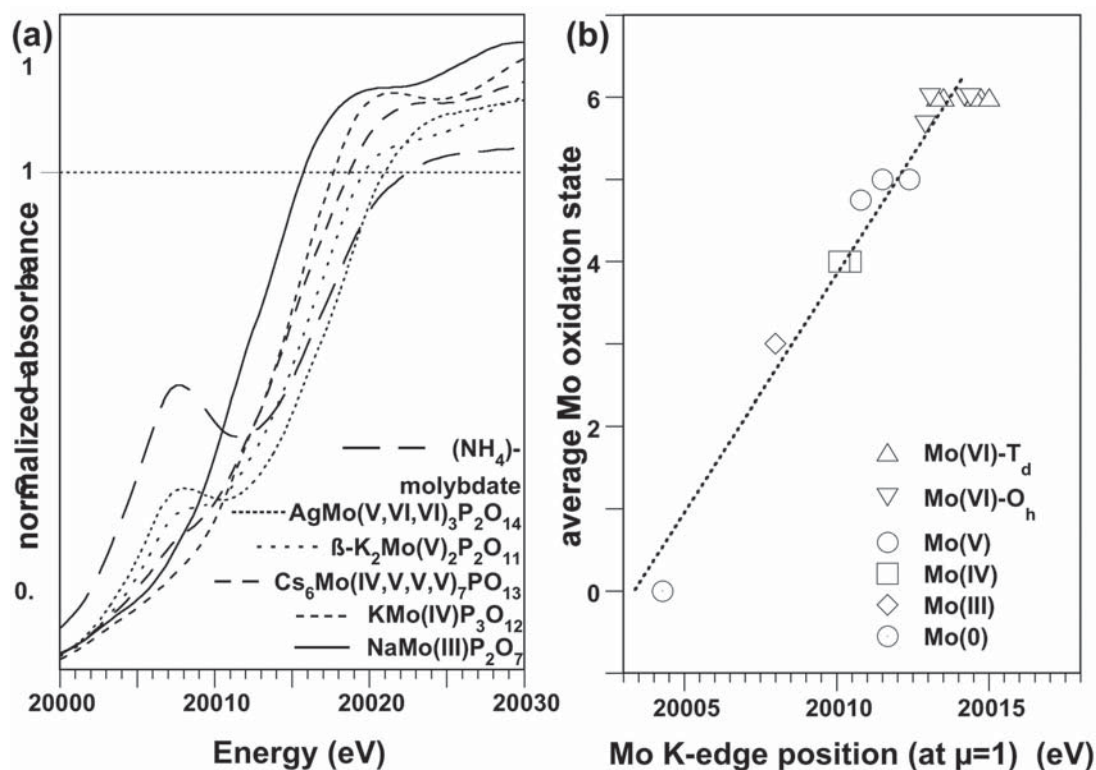


FIG. 4. Analysis of edge-energy position at the Mo *K*-edge. (a) Plot of the XANES for several model compounds, showing the relative complexity of that region. (b) Correlation between the average redox state of molybdenum as a function of the Mo *K*-edge position at $\mu = 1$ for various coordination-environments of Mo.

TABLE 4. COMPARISON OF THE Mo-O DISTANCES AND NUMBER OF NEIGHBORS FROM EXAFS DATA AND RESULTS OF X-RAY REFINEMENT

sample	EXAFS results					Data from X-ray refinement		
	shell	N	R (Å)	$\Delta\sigma^2$ (Å ²)	ΔE_0	N	R (Å)	Δd (Å)
CaMoO ₄	1-oxygen	3.9	1.77	1.2E-4	-0.7	4	1.77	0.02
MoO ₃	1-oxygen	1.5	1.72	2.17E-4	0 (f)	6	1.981	0.267
	2-oxygen	2.4	1.96	-1.05E-3	0 (f)			
	3-oxygen	2	2.32	1.23E-2	0 (f)			
	total	5.9	2.00	1.23E-1	0 (f)			
MoO ₂	1-oxygen	5.6	2.02	3.95E-4	3.43	6	2.011	0.045

f: fixed.

Back-scattering amplitude- and phase-shift functions from Na₂MoO₄·2H₂O.

the basis of this good agreement, the O back-scattering amplitude and Mo-O phase-shift functions extracted from sodium dimolybdate can be transferred to oxide-type compounds with Mo(IV) (such as MoO₂).

RESULTS ON GLASSES WITH SIMPLE COMPOSITION (AB, NS₂, AND NS₃) AS A FUNCTION OF OXYGEN FUGACITY

High-resolution molybdenum *K*-edge XANES spectra for Ab, NS₃, and NS₂ glasses (containing 400–2000 ppm molybdenum and synthesized with various values of oxygen fugacity) are presented in Figure 6a for glasses of albite composition (Ab), 6b for sodium disilicate (NS₂) glasses, 6c for sodium trisilicate (NS₃) glasses, and 6d for iron-bearing NS₃ glasses. Figure 6c (an inset in Fig. 6d) shows a close-up of the pre-edge feature for NS₃ glasses prepared at four different values of oxygen fugacity with and without 1 wt.% Fe. In all glasses synthesized in air, the pre-edge is intense and well resolved, suggesting the presence of major amounts of molybdate moieties. The molybdenum *K*-edge XANES spectra are unaffected until the oxygen fugacity (during synthesis) reaches $\sim 10^{-11}$ atm (Ab), $\sim 10^{-14}$ atm (NS₂), or $\sim 10^{-12}$ atm (NS₃) (the glasses become slightly brownish in color). Below these values of oxygen fugacity, the molybdenum *K*-edge XANES

spectra change rapidly within two log units of $f(\text{O}_2)$ to that typical of crystallites of metallic molybdenum (causing the glasses to become black). The presence of iron (present dominantly as ferrous iron, based on Fe K -edge XANES spectra) does not have a significant influence on the oxidation state of molybdenum in NS3 glasses.

Pre-edge analysis for these glasses (Fig. 7a) shows that most contain large amounts of molybdate moieties. More polymerized glasses, like Ab, show a significant shift in their pre-edge position, compared to NS3 glasses. Because the pre-edge data for Ab glasses plot close to the $^{141}\text{Mo(VI)}\text{--}^{161}\text{Mo(VI)}$ join, we conclude that only a minor amount of 6-coordinated Mo(VI) is present in these polymerized glasses. In contrast, the pre-edge data for glasses synthesized under lower fugacities of oxygen point to Mo(IV). The pre-edge information for

these reduced glasses is not well enough resolved to draw accurate conclusions on their molybdenum speciation. More information is required, as provided below.

ESTIMATION OF THE RELATIVE AMOUNTS OF Mo(V) IN AB AND NS3 GLASSES

X-band EPR spectra were collected at 295 K for several Ab glasses containing 500–2000 ppm molybdenum (Fig. 8). The normalized EPR spectra (Fig. 8a) are consistent with a g value of 1.94, typical of molybdenyl moieties (*i.e.*, $[\text{Mo(V)=O}]X_n$ units, with n from 3 to 6 and $X = \text{O, Cl, S}$; see Bobkova *et al.* 1989, Guesdon *et al.* 1994, 1995, Das *et al.* 1995). These units have two types of bonds, a short, double-bonded Mo=O with a distance near 1.7 Å, and three to six longer Mo–O bonds with distances between 1.85 and 2.2 Å (see also

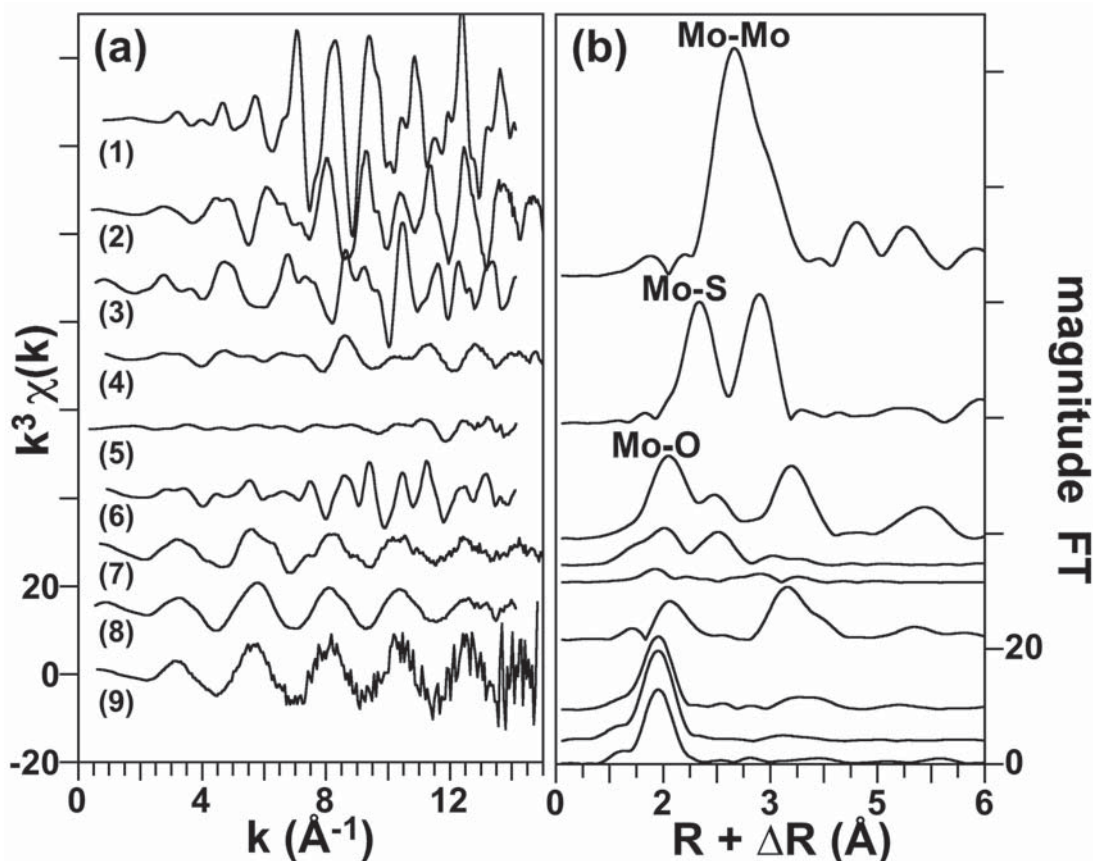


FIG. 5. Normalized k^3 -weighted EXAFS spectra for selected model compounds (a, left) and their Fourier transforms (b, right), showing the various Mo-pairs contributing to the spectra, according to structure refinements from the literature (see text). From top to bottom: (1) metallic molybdenum, (2) MoS_2 (molybdenite), (3) MoO_2 , (4) $\text{Mo}(\text{OC}_3\text{H}_7)_5$ (molybdenum isopropoxy), (5) ammonium dimolybdate, (6) MoO_3 (molybdite), (7) CaMoO_4 (powellite), (8) $\text{Na}_2\text{MoO}_4 \cdot 2\text{H}_2\text{O}$, and (9) Li_2MoO_4 .

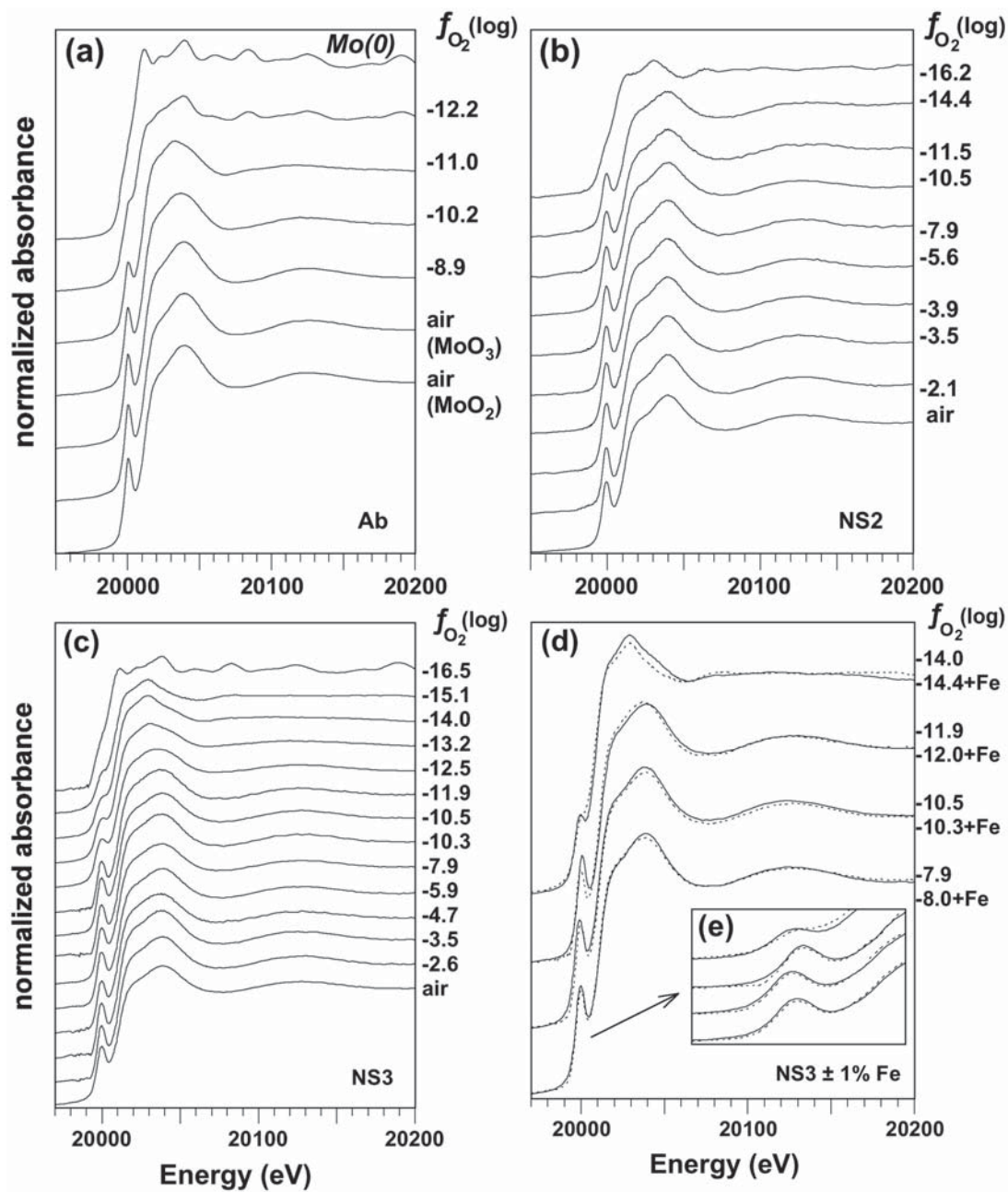


FIG. 6. High-resolution Mo *K*-edge XANES spectra for the glasses of that study, as a function of oxygen fugacity: (a) Ab, (b) NS2, (c) NS3 and (d) comparison of NS3 glasses (solid lines) with Fe-bearing NS3 glasses (dashed lines), and (e) close-up of the pre-edge feature for NS3 ± 1% Fe glasses.

McMaster *et al.* 2001) depending on the compound (similar to uranyl groups; see Farges *et al.* 1992). Analysis of the EPR spectra (Fig. 8b shows that the Mo(V) concentration is between 10 and 239 ppm in Ab glasses, and between 9 and 315 ppm in NS3 glasses (Table 5), which corresponds to a maximum of 9 mol.% of the total molybdenum present in the Ab glass synthesized at $10^{-10.3}$ atm (30 mol.% for NS3 glass prepared at $10^{-14.4}$ atm). In Ab glasses synthesized at lower fugacities of oxygen ($10^{-11.0}$ and 10^{-12} atm), the Mo(V) concentration is lower (as well as its relative importance). Similar results are obtained for NS3 glasses, but the maximum abundance of Mo(V) (29 atom %) is obtained for lower $f(\text{O}_2)$ values ($10^{-14.4}$ atm) as compared to Ab glasses. Hence, EPR spectroscopy suggests that Mo(V) is not the dominant species of molybdenum in these glasses, except in a very limited $f(\text{O}_2)$ range (1 log unit at most in the vicinity of 10^{-14} atm, such as the NS3 -14.4 glass, in which its proportion is approximately one-third.

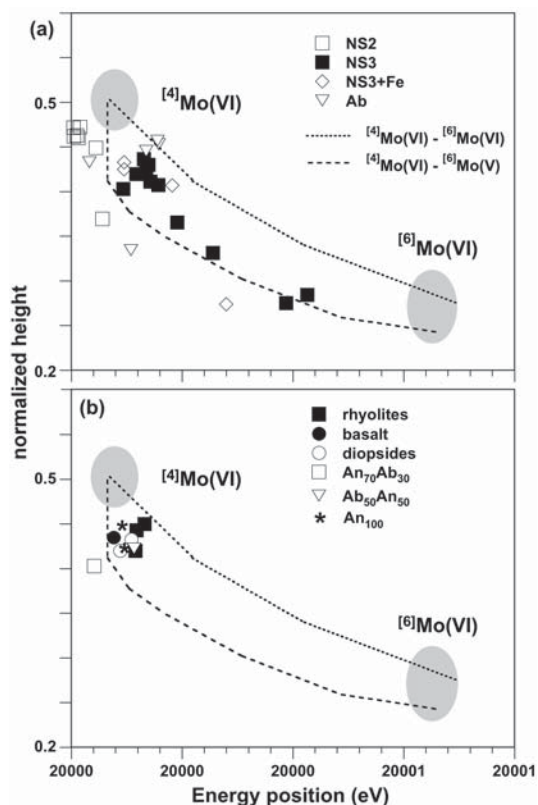


FIG. 7. Pre-edge information at the Mo *K*-edge for the glasses of this study, using the template for Figure 3b. (a) Glasses presented in Figure 6. (b) Glasses of more complex composition as well as glass of anorthite composition.

INFLUENCE OF THE OXYGEN FUGACITY ON THE EDGE POSITION

Figure 9a shows the variation in the edge position (at $\mu = 1$) for Ab, NS3, and NS2 glasses synthesized at $f(\text{O}_2)$ values ranging from that in air to 10^{-16} atm, and in Table 3, we present the redox results. The species Mo(VI) is abundant up to 10^{-10} atm for all compositions. Reduced oxidation-states appear at lower fugacities of oxygen. The transition to metallic molybdenum occurs over a small range of oxygen fugacities. The Ab glasses are reduced more easily than NS2 or NS3 glasses. For the NS3 series, we calculated the relative abundance for each oxidation state of molybdenum as a function of $f(\text{O}_2)$ based on the XAFS and EPR informa-

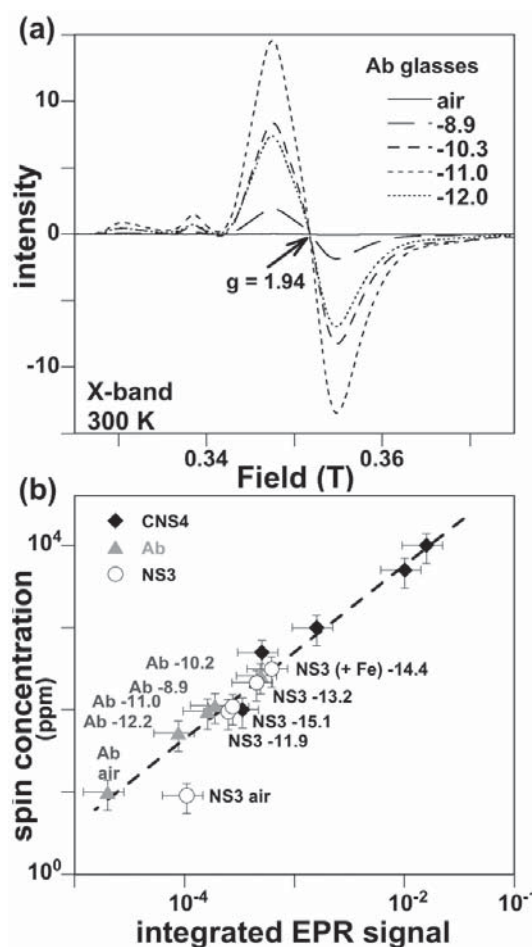


FIG. 8. EPR information for selected glasses. (a) Normalized integrated EPR spectra collected at 300 K. (b) Correlation between the integrated EPR spectra and the spin concentration calibrated for Cu^{2+} -bearing CNS4 glasses and Ab and NS3 glasses.

tion (Fig. 9b). We did not consider Mo(III) because we did not observe any EPR evidence for this oxidation state in any of the glasses studied. For example, the NS3 glass synthesized at $10^{-16.5}$ atm has an edge position that suggests an average redox state of molybdenum of 2.6. However, its XANES spectrum suggests the presence of large amounts of metallic molybdenum, indicating that the oxidized form of molybdenum must be Mo(IV). Figure 9b shows that losses of molybdenum to the crucible were important for the NS3 melt below NNO + 1, as molybdenum can form alloys with the platinum of the crucibles used. In addition, examination of Figure 9b

suggests that molybdenum is much less soluble in melts under reducing conditions than in air (the most reduced glasses show XANES spectra typical of crystalline molybdenum metal, indicating some saturation of molybdenum in the glasses). This behavior of molybdenum follows that observed for other metals such as the actinides [see Farges *et al.* (1992) and references therein]. Figure 9b also shows that Mo(VI) is dominant until relatively low values of oxygen fugacity (near the IW buffer). Around the IW buffer, the solubility of molybdenum is affected by the increasing abundance of Mo(V). In contrast, reduced molybdenum species [Mo(V) and Mo(IV)] exist only for a limited range of oxygen fugacities (IW-1 to IW-3). For Ab, metallic molybdenum precipitates at 10^{-12} atm/1300°C, which is also approximately equivalent to IW-3.

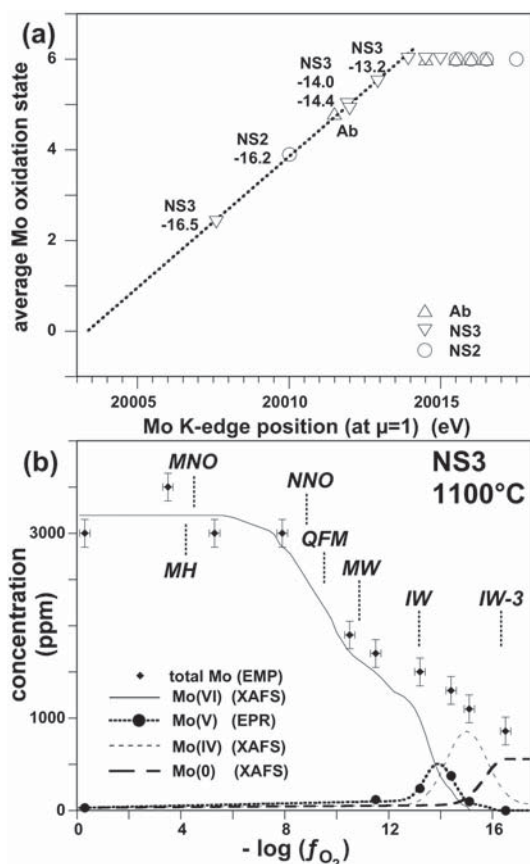


FIG. 9. Redox determinations in glasses of Ab, NS2 and NS3 composition. (a) Analysis of edge-energy position at the Mo K-edge for Ab, NS2 and NS3 glasses, using the template from Figure 4b. (b): Estimation of the relative amounts of each oxidation state of Mo as a function of oxygen fugacity. The decrease in the concentration of Mo (originally 3000 ppm for all glasses, synthesized from the same batch, prior reduction *in situ*) is related to losses of Mo to the platinum crucible. Acronyms in italics (MNO, NNO, QFM, MW, IW) refers to oxygen fugacity buffers.

XANES STUDIES OF MORE COMPLEX GLASSES

Figure 10 shows high-resolution molybdenum K-edge spectra collected for a set of glasses of more complex compositions (basaltic, rhyolitic, Ab_xAn_y) as well for three glasses of diopside composition. All glasses show an intense pre-edge feature indicative of molybdate moieties, as confirmed by the analysis of their pre-edges (Fig. 7b). Some of these glasses have a dark brownish color (such as DI -7.0 and DI -8.9) due to the presence of molybdenyl moieties [*i.e.*, Mo(V)], which is confirmed by their pre-edges (Fig. 7b). However, this information suggests that

TABLE 5. INFORMATION ON THE ELECTRON PARAMAGNETIC RESONANCE (EPR) SPECTRA OF THE MODEL Cu(II)-BEARING GLASSES (NCS5) AND SELECTED Mo-BEARING GLASSES

Glass sample	Integrated EPR spectra (0.32-0.38 Tesla)	Cu(II) or Mo(V) spin concentration	% of total Mo as Mo(V) ²
NCS5 glass with			
100 ppm Cu(II)	0.000337	100	-
500 ppm Cu(II)	0.000506	500	-
1000 ppm Cu(II)	0.001595	1000	-
5000 ppm Cu(II)	0.010121	5000	-
10000 ppm Cu(II)	0.015950	10000	-
Ab glasses			
air	0.000020	10 ¹	< 1
10 ^{-8.9}	0.000190	113 ¹	6
10 ^{-10.3}	0.000492	239 ¹	9
10 ^{-11.0}	0.000162	96 ¹	6
10 ^{-12.0}	0.000088	52 ¹	2
NS3 glasses			
air	0.000105	9 ¹	< 1
10 ^{-11.5}	0.000250	95 ¹	7
10 ^{-13.2}	0.000451	214 ¹	16
10 ^{-14.4}	0.000620	315 ¹	29
10 ^{-15.1}	0.000274	109 ¹	9
average error	0.000005	5	3

¹ calculated based on the information for Cu-bearing NCS4 glasses.

² based on electron-microprobe information for total Mo (from Table 2).

Mo(V) comprises no more than ~20 atom % of the total molybdenum, which is dominantly represented as "colorless" molybdate moieties. The last DI glass (DI -10.0) is black. Its X-ray diffraction and its XANES spectrum are typical of crystalline metallic molybdenum, indicating that molybdenum saturation occurred in that melt when the oxygen fugacity dropped below $10^{-8.9}$ atm. In the Ab_xAn_y glasses ($0 < x < 100$, $y = 100 - x$), the molybdenum *K*-edge XANES spectra are little affected by changes in $f(O_2)$, showing major amounts of molybdate moieties. Hence, there is little difference in the molybdenum speciation as a function of glass composition, until atoms of non-bridging oxygen are present to stabilize Mo(VI) as molybdate (and molybdenyl) moieties and until the oxygen fugacity exceeds the IW buffer.

EXAFS SPECTRA OF SELECTED MO-BEARING GLASSES

Figure 11 shows the k^3 -weighted normalized EXAFS spectra and their Fourier transforms calculated for a selection of glasses presented above. Figures 11a, c, and e also show the best model calculated for each glass (except the most reduced glasses, in which metallic

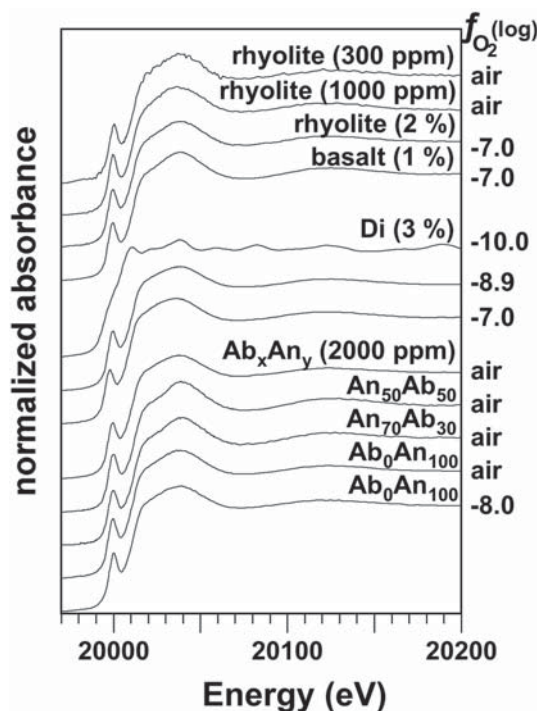


FIG. 10. High-resolution Mo *K*-edge XANES spectra for glasses of more complex composition, showing the presence of pre-edge features, related to molybdate moieties.

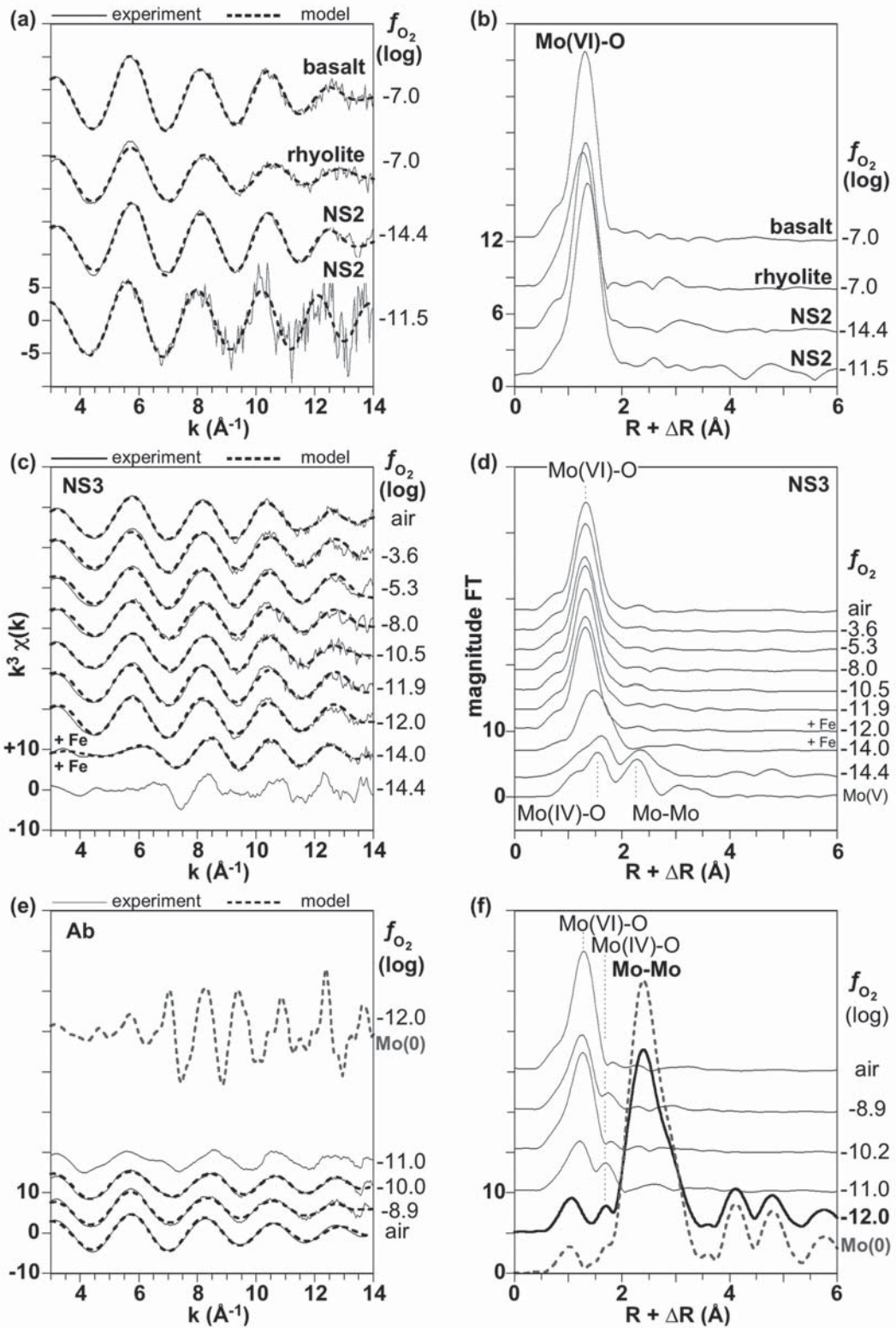
molybdenum precipitates occur). Their corresponding FT (Figs. 11b, d, and f) show that all glasses synthesized under ambient or moderately reducing conditions have mostly one-pair correlation arising from oxygen first neighbors. The results of least-squares modeling of the EXAFS data for these glasses are given in Table 6. These results confirm that Mo(VI) in these oxidized glasses is mainly four-coordinated, with average Mo–O distances of 1.76(2) Å. No other significant contribution is observed around molybdenum, including that arising from next-nearest silicon or molybdenum neighbors. This observation suggests that molybdenum was dissolved in the melts prior to the quench and that MoO₄ units are not connected to the tetrahedral framework. In the reduced NS3 glass synthesized at $10^{-14.4}$ atm (Table 6, Figs. 11c, d), a double oxygen shell was needed to model the EXAFS data for this sample, as suggested by its Fourier Transform (Fig. 11d). On the basis of Figure 9b, we attribute this environment to the presence of both Mo(V) and Mo(IV) in the proportion $^{2/3} : ^{1/3}$. This environment is close to that measured for molybdenyl moieties in β -K₂Mo(V)₂O₄P₂O₇ [compare with Figs. 5a, b, spectrum (5)]. Finally, in the most reduced glasses (such as "Ab -12.0"), the FT of molybdenum is nearly identical to that for crystalline MoO, confirming that metallic molybdenum precipitated from the melt.

DISCUSSION

Importance of molybdate moieties in reduced, anhydrous glasses

The results obtained from XAFS and EPR spectroscopies show that molybdenum exists mostly as molybdate moieties in the large majority of the silicate glasses examined in this study, in agreement with X-ray photoelectron spectroscopy (XPS) and XAFS measurements on other Mo-containing silicate glasses (Nyholm & Werme 1981, Petit-Maire 1988, Kuzmin & Purans 1997, Rocca *et al.* 1999). These molybdate moieties are similar to those observed in various crystalline alkali and alkaline earth molybdates, such as Na₂MoO₄•2H₂O. Surprisingly, these molybdate units remain the dominant form of molybdenum until relatively low $f(O_2)$

FIG. 11. Normalized k^3 -weighted EXAFS spectra for selected glasses (a,c,e) as compared to their Fourier transforms (b,d,f), showing the presence of molybdate moieties at most oxygen fugacities, except in reduced glasses, where molybdenyl moieties (NS3 -14.4) or metallic polycrystalline molybdenum (Ab -12.0) are present. For most EXAFS, the best model calculated is shown as a dashed line over the experimental spectra.



conditions (*i.e.*, until the IW buffer), whatever the melt polymerization (with NBO/T comprised between 0 and 1 as in Ab, NS3 and NS2). Replacing network modifiers (*i.e.*, alkalis *versus* alkaline earths) or adding moderate amounts of iron (1 wt.%) has little influence on the molybdenum speciation and its connectivity to the framework of tetrahedra. Simple bond-valence models (see Farges *et al.* 1990, 1991 for details) suggest that the average $^{14}\text{Mo(VI)}\text{-O}$ bond valence is ~ 1.5 valence units (*vu*). Because this bond valence is so high, $^{14}\text{Mo(VI)}$ cannot bond to any type of bridging oxygen atoms; otherwise, the sum of bond valences around the connecting oxygen atoms would greatly exceed the bond-valence sum (2.0 ± 0.1 *vu*) required by Pauling's second rule (Pauling 1929). In contrast, $^{60}\text{Mo(VI)}$ is predicted to bond only to oxygen atoms bonded to two or three network modifiers (see Fig. 12), as in crystalline molybdates. Consequently, we cannot predict from the present dataset if molybdenum could bond preferentially to alkalis (such as Na) or alkaline earths (such as Ca). However, because of their greater bond-valence (Brown *et al.* 1995), bonding to alkaline earths would require about half the number of network modifiers to charge-compensate molybdenum as would alkalis atoms.

Localization of molybdenum in silicate glasses

Because molybdenum was introduced as MoO_3 in all glasses (except one Al composition), each molybdenum atom added to the melt was accompanied by three non-bridging atoms of oxygen (in crystalline MoO_3 , each O atom is shared with three molybdenum atoms; Kihlberg 1963). In calcic glasses, two Ca atoms are needed, as Ca^{2+} charge-balance more efficiently than the monovalent alkalis. In most of the glass composi-

tions studied, NBO atoms are much more abundant than molybdenum, providing a large excess of NBO atoms to which molybdenum preferentially bonds. This explains why, in supercooled melts, Mo(VI) can follow its thermodynamic affinity for tetrahedral geometries [molybdates are the most common Mo(VI) -bearing minerals]. In highly polymerized glasses, an excess of NBO atoms is not available, making the bonding of molybdenum more difficult. In these glasses, molybdenum is also present as MoO_6^{6-} polyhedra, most likely as a result of the shortage of NBO atoms. One efficient way for Mo(VI) to adapt to this shortage is to decrease its bond valence with oxygen atoms in order to make it more "connectable" to the other types of oxygen atoms, such as bridging oxygen atoms in the framework of tetrahedra. At constant redox state, Mo(VI) must then increase its coordination to 6, which results in a drop in bond valence from 1.5 to 1.0 *vu*. In this case, Mo(VI)O_6^{6-} units can connect to network formers by consuming the remaining NBO atoms or by destabilizing some bridging oxygen atoms of the framework of tetrahedra. Another possibility for molybdenum is to form enriched domains, which must be close in structure to molybdate [equivalent to a thermodynamic saturation in the " MoO_3 " (or " MoO_2 ") component(s); see Stemprok & Voldan 1974, Ryabchikov *et al.* 1981]. This model explains why only some MoO_6^{6-} units are observed in Ab glasses (whether molybdenum saturated or not). Similar mechanisms of saturation have been observed for other highly charged cations (see Farges *et al.* 1991), but the unusually high valence of Mo(VI) makes the solubility mechanism of such a transition element even more unique. On the other hand, bond valence also explains why metallic molybdenum is not soluble in fully polymerized glasses (we attempted to dissolve trace amounts of metallic molybdenum at 2500°C in a silica melt without any success).

Reduced states of Mo

Less direct information is obtained for the reduced states of molybdenum (namely V and IV), because of the impossibility to find an oxygen fugacity that would "isolate" either of these redox states. However, owing to EPR measurements, Mo(V) is detected in relatively reduced glasses (particularly the non-fully-polymerized ones such as NS2 and NS3), and its signal is consistent with the presence of molybdenyl moieties. These molybdenyl moieties are characterized by a short, apical, covalent and double-bonded Mo=O bond (connecting dimers) and five "equatorial", longer, less strongly covalent and single-bonded Mo-O bonds (Cotton & Wilkinson, 1988). The bond valence of the longer Mo-O bonds is ~ 0.7 *vu* (O'Keeffe & Brese 1992). These relatively high bond-valences require Mo(V) to bond to an important number of non-bridging oxygen atoms, which also makes Mo(V) a network modifier in oxide melts (as for Ta and Nb). Concerning Mo(IV) ,

TABLE 6. EXAFS DATA-REDUCTION PARAMETERS FOR THE Mo-O PAIR IN SELECTED NS3 GLASSES

sample	shell	EXAFS analysis					χ^2 *
		N	R (Å)	$\Delta\sigma^2$ (Å ²)	ΔE_0		
NS3 -0.7	1-oxygen	4.1	1.77	-2.08E-4	-0.408	8.6E-4	
NS3 -3.6	1-oxygen	4.1	1.76	-1.54E-4	-0.913	1.35E-3	
NS3 -5.3	1-oxygen	3.8	1.75	-1.16E-4	-1.908	5.22E-3	
NS3 -7.9	1-oxygen	4.0	1.76	-4.51E-4	-1.357	2.69E-3	
NS3 -10.5	1-oxygen	4.0	1.76	-5.34E-4	-0.996	1.96E-3	
NS3 -11.9	1-oxygen	3.9	1.75	-4.42E-4	1.547	5.37E-3	
NS3 -14.4	1-oxygen	1.9	1.74	3.19E-4	0(f)		
	1-oxygen total	3.3	2.06	3.57E-3	0(f)		4.81E-3
average error		0.4	0.02	2.00E-4	0.5		

f: fixed parameter (to minimize the number of correlated parameters). Amplitude- and phase-shift from $\text{Na}_2\text{MoO}_4 \cdot 2\text{H}_2\text{O}$. Anharmonic third cumulant parameter (C^3) converged to zero for all models. * Chi-square of the least-squares fit to the data.

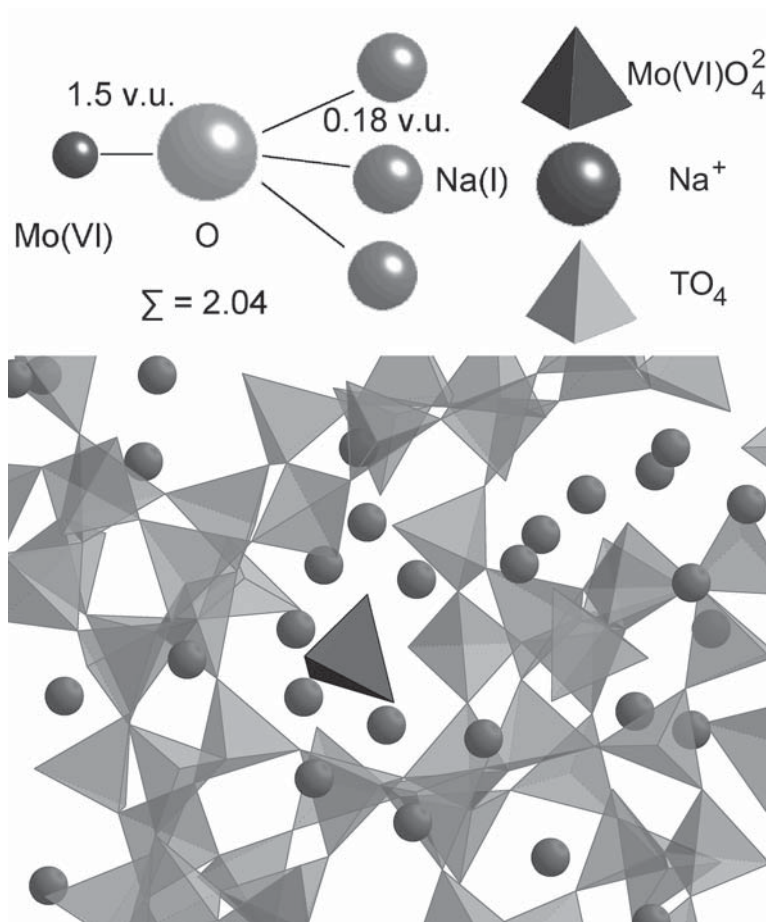


FIG. 12. Example of the structure of a NS3 glass containing a molybdate moiety, respecting Pauling's bond-valence rules, *i.e.*, the oxygen atoms of the MoO_4^{2-} group are connected to Na second neighbors in the areas of the glass enriched in network modifiers.

the absence of a pre-edge in the most strongly reduced glasses (such as NS3 at $10^{-15.1}$ atm) suggests that tetravalent molybdenum is more likely to form moieties close to these found in MoO_2 (octahedral) instead of tetrahedral or square pyramidal moieties (which would result in a detectable pre-edge feature and shoulder before the main *K*-edge of molybdenum). Thus, Mo(IV) behaves also as a "weak" network modifier, like Zr (Farges *et al.* 1991). Based on EPR spectroscopy, there is no evidence for Mo(III) in any of our glasses. This would also exclude the presence of Mo(II), suggesting that Mo(IV) reduces directly to Mo(0) in only a few log units of oxygen fugacity.

Medium-range environments of molybdenum

We found no experimental evidence for next-nearest atoms of aluminum, silicon, or molybdenum neighbors around Mo in most of the glasses investigated in this study, which can be rationalized using Pauling's second and third rules. As outlined previously, molybdenum is present mostly as molybdate units, making this element unable to bond to bridging oxygen atoms (Fig. 12 top). For instance, in NS3 glass, Pauling's second and third rules suggest that molybdate groups should bond (ideally) to 3 NaO_6 polyhedra through edge-shared polyhedra. In Figure 12 (bottom), we present a struc-

tural model of a NS3 glass with a molybdate moiety that is located in a “cavity” inside the framework of tetrahedra (or in a sodium-rich portion of the glass), respecting stoichiometry and structural constraints defined above. On the basis of this model, we calculated an *ab initio* EXAFS spectrum using FEFF 7.02 (Ankudinov *et al.* 1998). We did not observe any clear evidence for second-neighbor Na atoms, because their contributions were too disordered to be significant, in agreement with the experiment (molybdenum-bearing glasses and crystalline $\text{Na}_2\text{MoO}_4 \cdot 2\text{H}_2\text{O}$). However, bond-valence considerations suggest that network modifiers (such as alkali and alkaline earths) are the key elements to dissolve molybdenum in glasses. In addition, these models explain why molybdate crystals nucleate easily from silicate glasses (such as powellite in Ca-rich compositions; Petit-Maire 1988), because of the close structural relationships between cation coordination and nucleation (Müller *et al.* 1992).

Speciation and solubility

In silicate glasses and melts, molybdenum-solubility curves show two “regimes” that are interpreted in terms of Mo(VI) and Mo(IV), in proportion to relative abundance (Hillgren 1993, Holzheid *et al.* 1994, O’Neill & Eggins 2002). On the basis of these models, these investigators agree that the first regime (which predominates at high values of oxygen fugacity) corresponds to the presence of Mo(VI). The second regime is attributed to Mo(IV), which is assumed to become predominant below the iron-wüstite (IW) buffer. However, none of these investigators considered the structural information yet available for molybdenum in oxide glasses (see Camara *et al.* 1979, Horneber *et al.* 1982, Petit-Maire 1988, Farges *et al.* 1990, Sawaguchi *et al.* 1996, Siewert *et al.* 1997a, b, Durasova *et al.* 1998, 1999). For instance, EPR information has demonstrated the presence of dominant amounts of Mo(V) in all molybdenum-bearing glasses prepared under reducing conditions. Also, the presence of highly reduced redox states of molybdenum such as Mo(III) and Mo(II) also requires some discussion. Our study shows that Mo(V) is predominant [together with Mo(VI) and Mo(IV)] near the IW buffer. In contrast to Mo-bearing phosphate glasses (see Camara *et al.* 1979, Horneber *et al.* 1982, Short *et al.* 2005), Mo(III) has not been detected by EPR in our silicate and aluminosilicate glasses; Durasova *et al.* (1998, 1999) reached similar conclusions. The presence of Mo(II) is still not yet fully established in oxide glasses, but its consideration is still needed, although its occurrence seems to have quite a limited range of $f(\text{O}_2)$ conditions [within one log unit of $f(\text{O}_2)$]. Hence, the available models on solubility of molybdenum must be fully revisited in light of the past and present direct sets of spectroscopic information, particularly for Mo(V).

In agreement with Holzheid *et al.* (1994) and O’Neill & Eggins (2002), the solubility of molyb-

denum in NS3 melt (Fig. 9b) begins to be affected at low values of oxygen fugacity, namely near $\sim\text{IW}-1$ and $\text{IW}-2$ (see Fig. 9b). These conditions of oxygen fugacity correspond (in this study) to where Mo(IV) becomes the dominant form of molybdenum. Consequently, the first regime of molybdenum solubility at relatively high values of oxygen fugacity (*i.e.*, air to $\text{IW}-1$) corresponds to the stability domain of both Mo(VI) and Mo(V). Interestingly, Mo(VI) and Mo(V) forms molybdate and molybdenyl moieties, which are characterized by the presence of highly covalent Mo–O bonds (Cotton & Wilkinson 1988). In contrast, Mo(IV) forms less covalent bonds, as a weak network modifier. Finally, we also note that the second regime of solubility ($\text{IW}-1$ to $\text{IW}-4$) corresponds also to the range of oxygen fugacity for which metallic molybdenum precipitates from the melt.

On the concept of “complexes” around molybdenum

So-called “complexes” of molybdenum with silicon (Isuk & Carman 1981, 1983) or calcium (O’Neill & Eggins 2002) have been invoked to explain the geochemical behavior and the solubility data of molybdenum in oxide melts. Such large molecular entities would require too much energy to exist as such in oxide melts without oxide melts interacting with the framework of tetrahedra. Thus, the structure and thermochemistry are better explained with the concepts of network formers and modifiers (Brown *et al.* 1995, Stebbins 1995). A simpler (and energetically more favorable) model is to consider that network modifiers (such as sodium or calcium) will “provide” some non-bridging oxygen atoms (NBO) required for each of the molybdenum redox states to be stabilized (Farges 1995), as verified by molecular dynamics simulations (Le Grand 1999). In the case of Mo(VI), three atoms of calcium are required around the central molybdenum (and no network former; Fig. 12), forcing molybdenum to migrate in the relatively depolymerized domains of the oxide glass or melt (Farges 1995, Siewert *et al.* 1997a,b, Le Grand 1999, Calas *et al.* 2003). This model explains why calcium molybdate (powellite) also nucleates in calcic glasses without drastic thermal reorganization of the structure of the supercooled melt.

Using the same bond-valence considerations, no “complexes” are required around Mo(IV), as this cation behaves as a network modifier: the oxygen atoms around Mo(IV) are predicted to bond simultaneously to network modifiers and formers, exactly as Zr in similar silicate glass or melts (Farges *et al.* 1991). Consequently, large structural differences are found between Mo(VI), Mo(V) and Mo(IV). This change in bonding requirements does not require any indirect complexation model, as it fits well within the description of the network of tetrahedra invoked currently for oxide glasses and melts (Fig. 12). Also, this model sheds a new light the solubility of molybdenum. The solubility

of molybdenum is not explained in terms of a 6-to-4 redox change, but more because of a deeper change in bonding requirements of molybdenum (from highly covalent to less covalent). Consequently, the “ionic” or “complex” approach to solubility must be replaced by a newer and more robust concept that is more relevant to oxide melt structure and dynamics, *i.e.*, by considering the way each of the moieties around each ion (when dissolved in the oxide melt) interacts with the framework of tetrahedra. In other words, the solubility is not controlled by “static and isolated” ions, but rather by a change in connectivity of the molybdenum in various redox states in the melt.

Implications for the activity coefficients of Mo(IV) in melts

Understanding solubility requires some knowledge of the activity coefficients of molybdenum in oxide melts (O'Neill & Eggins 2002). In the presence of mixed redox states of molybdenum, titanium has been used by these authors as a structural analogue of molybdenum in an effort to extrapolate the activity coefficients that are required to model solubility information. Not surprisingly, large differences exist between Mo(IV) and Ti(IV) in oxide glass and melts. First, the former is dominantly five-coordinated in NS2, NS3 and glasses of albite composition (as titanyl moieties, which show a network-forming character, together with a highly covalent Ti=O bond; Farges *et al.* 1996). No such “molybdyl” units are known for Mo(IV) (Cotton & Wilkinson 1988), and we found no EXAFS evidence on their presence in our glasses. Instead, on the basis of our XANES information, despite the limitation of resolution, we predict that Mo(IV) probably forms poorly distorted geometries such as octahedra (close to these observed in MoO₂; see Fig. 7b). These differences suggest then large differences in the ionic radius of ¹⁵¹Ti(IV) and ¹⁶¹Mo(IV) (*i.e.*, 0.51 and 0.65 Å, respectively; Shannon & Prewitt 1969). Also, Ti(IV) is a well-described network-former, whereas Mo(IV) is a network modifier. Hence, these large differences prevent the extrapolation of accurate activity-coefficients for Mo(IV), based on those for Ti(IV). Following this reasoning, zirconium would then be a much better “analogue” for Mo(IV) in terms of activity coefficients. This aspect shows how structural studies on glass and melt, despite their own intrinsic limitations, are helpful in formulating thermochemical models.

Geochemical implications

The local structure around molybdenum in silicate glasses of simple composition as well as in more complex compositions (*i.e.*, basaltic or rhyolitic compositions that mimic natural magmas) is similar. The polymerization of tetrahedra (as assessed by NBO/T values) is a much more important parameter, resulting

in highly coordinated molybdenum environments such as ¹⁶¹Mo(VI), which may be an indicator of presaturation of the melt in the MoO₃ component. Hess (1991) provided a detailed description of these saturation concepts. Molybdenum remains highly soluble until non-bridging atoms of oxygen (accompanying network modifiers) are present. This result is similar to that for other highly charged cations (or high-field-strength elements), such as Zr and Ti (Farges & Brown 1997, Farges & Rossano 2000), despite the network-forming character of Ti. The influence of iron is negligible until Mo(VI) dominates. At lower values of oxygen fugacity, where Mo(IV) dominates, our data show some slight (merely significant) differences in molybdenum speciation that could possibly indicate a weak redox equilibria between it and iron. More studies are needed to investigate this aspect as the stability domain for Mo(IV) is relatively narrow.

This reasoning would seem to suggest that simple glasses can be considered as structural analogues of natural magmas. However, the evidence of a large field of stability for Mo(VI) is at variance with expectations from mineralogical observations, which indicate that molybdenite [Mo(IV)S₂] is the major Mo-containing mineral in the Earth's crust. This discrepancy indicates that other parameters, such as pressure, temperature, fluids (halogens and H₂O), as well as potential complexing anions (*e.g.*, S), play a more important role than oxygen fugacity in determining the dominant speciation of molybdenum in crustal rocks, in which fluids are known to play a critical role. We will examine the effects of these other parameters on the speciation of molybdenum in the companion paper (Farges *et al.* 2006) and will show that they have a dramatic influence.

ACKNOWLEDGEMENTS

We thank Harald Behrens (University of Hanover) for providing glass of albite composition, the staff of SSRL (Stanford, California) for their help for data collection. Robert Linnen, Andrew Berry and Don Baker for their constructive comments on the manuscript. The Deutsche Forschung Gesellschaft is also thanked for its generous financial support to RS as well as the EEC TMR network “Water in molten silicates”. The Stanford Synchrotron Radiation Laboratory is supported by the DOE, Office of Basic Energy Sciences, and NIH, Biotechnology Resource Program, Division of Research Resources. This study was supported by CNRS (Farges) and in part by NSF Grant CHE-0431425 (Brown).

REFERENCES

- ADELSON, J.M., HELZ, G.R. & MILLER, C.V. (2001): Reconstructing the rise of recent coastal anoxia; molybdenum in Chesapeake Bay sediments. *Geochim. Cosmochim. Acta* **65**, 237-252.

- ALEKSANDROV, V.B., GORBATI, L.V. & ILJUHIN, V.V. (1967): The crystal structure of powellite. *Kristallografiya* **13**, 512-513 (in Russ.).
- ANKUDINOV, A.L., RAVEL, B., REHR, J.J. & CONRADSON, S.D. (1998): Real-space multiple-scattering calculation and interpretation of x-ray absorption near-edge structure. *Phys. Rev. B* **58**, 7565-7576.
- AVERBUCH-POUCHOT, M.T. (1988): Structure of an ammonium molybdenyl diphosphate: $(\text{NH}_4)_2\text{MoO}_2\text{P}_2\text{O}_7$. *Acta Crystallogr.* **44**, 2046-2048.
- BAI, T.B. & KOSTER VAN GROOS, A.F. (1999): The distribution of Na, K, Rb, Sr, Al, Ge, Cu, W, Mo, La, and Ce between granitic melts and coexisting aqueous fluids. *Geochim. Cosmochim. Acta* **63**, 1117-1131.
- BENDOR, L. & SHIMONY, Y. (1974): Crystal-structure, magnetic-susceptibility and electrical-conductivity of pure and NiO-doped MoO_2 and WO_2 . *Mater. Res. Bull.* **9**, 837-844.
- BLASSE, G. (1968): Crystal structure and fluorescence of compounds $\text{Ln}_2\text{Me}^{4+}\text{Me}^{6+}\text{O}_8$. *J. Inorg. Chem.* **30**, 2061-2099.
- BOBKOVA, N.M., RAKOV, I.L. & SOLOVEI, N.P. (1989): Spectroscopic study of molybdenum-containing glass structure. *J. Non-Crystal. Solids* **111**, 98-102.
- BOGATIKOV, O.A., GORSHKOV, A.I., MOKHOV, A.V., ASHIKHMINA, N.A. & MAGAZINA, L.O. (2001): The first finding of native molybdenum, silver sulfide, and iron-tin alloy in the lunar regolith. *Geochem. Int.* **6**, 604-608.
- BOOKSTROM, A.A. (1999): Molybdenum. In *The Encyclopedia of Geochemistry* (C. Marshall & R.W. Fairbridge, eds.). Chapman and Hall, New York, N.Y. (412-413).
- BOUDLICH, D., HADDAD, M., NADIRI, A., BERGER, R. & KLIAVA, J. (1998): Mo^{5+} ions as EPR structural probes in molybdenum phosphate glasses. *J. Non-Crystal. Solids* **224**, 135-142.
- BROUDER, C. (1990): Angular dependence of X-ray absorption spectra. *J. Phys. Condens. Matter* **2**, 701-738.
- BROWN, G.E., JR., CALAS, G., WAYCHUNAS, G.A. & PETIAU, J. (1988): X-ray absorption spectroscopy: applications in mineralogy and geochemistry. In *Spectroscopic Methods in Mineralogy and Geology* (F.C. Hawthorne, ed.). *Rev. Mineral.* **18**, 431-512.
- BROWN, G.E., JR., FARGES, F. & CALAS, G. (1995): X-ray scattering and X-ray spectroscopy studies of silicate melts. In *Structure, Dynamics and Properties of Silicate Melts* (J.F. Stebbins, P.F. McMillan & D.B. Dingwell, eds.). *Rev. Mineral.* **32**, 317-410.
- CALAS, G. (1981): Spectroscopic effects of molybdenum contamination from containers. *U.K. Nat. Environment Res. Council, Prog. Experim. Petrol.* **5**, 109-112.
- CALAS, G. (1988): Electron paramagnetic resonance. In *Spectroscopic Methods in Mineralogy and Geology* (F.C. Hawthorne, ed.). *Rev. Mineral.* **18**, 431-512.
- CALAS, G., LE GRAND, M., GALOISY, L., & GHALEB, D. (2003) Structural role of molybdenum in nuclear glasses: an EXAFS study. *J. Nucl. Mater.* **322**, 15-20.
- CALAS, G. & PETIAU, J. (1983): Structure of oxide glasses. Spectroscopic studies of local order and crystallochemistry. Geochemical implications. *Bull. Minéral.* **106**, 33-55.
- CAMARA, B., LUTZE, W. & LUX, J. (1979): An investigation of the valency state of molybdenum in glasses with and without fission products. In *Scientific Basis for Nuclear Waste Management II* (C.M.J. Northrup, Jr., ed.). Plenum Press, New York, N.Y. (93-102).
- CANDELA, P.A. (1989): Felsic magmas, volatiles, and metallogenesis. In *Ore Deposits Associated with Magmas* (J.A. Whitney & A.J. Naldrett, eds.). *Rev. Econ. Geol.* **4**, 223-233.
- CANDELA, P.A. (1997): A review of shallow, ore-related granites: textures, volatiles, and ore metals. *J. Petrol.* **38**, 1619-1633.
- CANDELA, P.A. & BOUTON, H.D. (1990): The influence of oxygen fugacity on tungsten and molybdenum partitioning between silicate melts and ilmenite. *Econ. Geol.* **85**, 633-640.
- CANDELA, P.A. & HOLLAND, H.D. (1984): The partitioning of Cu and Mo between silicate melts and aqueous fluids. *Geochim. Cosmochim. Acta* **48**, 373-380.
- CANDELA, P.A. & HOLLAND, H.D. (1986): A mass transfer model for copper and molybdenum in magmatic hydrothermal systems: origin of the porphyry-type ore deposit. *Econ. Geol.* **81**, 1-19.
- CARTEN, R.B., WHITE, W.H. & STERN, H.J. (1993): High-grade granite-related molybdenum systems: classification and origins. In *Mineral Deposit Modeling* (R.V. Kirkham *et al.*, eds.). *Geol. Assoc. Can., Spec. Pap.* **40**, 521-554.
- COTTON, F.A., & WILKINSON, G. (1988): *Advanced Inorganic Chemistry*. John Wiley International, New York, N.Y.
- COZAR, O., ARDELEAN, I., SIMON, S. & DAVID, L. (1993): ESR studies of Mo^{5+} ions in potassium-borate and soda-phosphate glasses. *Solid State Commun.* **85**, 461-465.
- DAS, B.B., CONSTANTIN, G., BOREL, M.M., GRANDIN, A., LECLAIRE, A. & RAVEAU, B. (1995): EPR studies on molybdenum phosphates $\text{Mo}_2\text{P}_4\text{O}_{15}$, $\text{NaMo}_3\text{P}_3\text{O}_{16}$ and $\text{BaMo}_2\text{P}_4\text{O}_{16}$ in the temperature range 300-4.2 K. *Bull. Mater. Sci.* **18**, 125-131.
- DRÄGER, G., FRAHM, R., MATERLIK, G. & BRUMMER, O. (1988): On the multipole character of the x-ray transitions in the pre-edge structure of Fe K absorption spectra. *Phys. Status Sol. B*, **146**, 287-293.

- DURASOVA, N.A., BELYAEVA, V.K., KOCHNOVA, L.N. & RYABCHIKOV, I.D. (1999): Speciation and transport properties of molybdenum in synthetic glass analogues of igneous rocks. *Geokhim.*, 653-657 (in Russ.).
- DURASOVA, N.A., BELYAEVA, V.K., KOCHNOVA, L.N., TRONEVA, M.A., & BANNYKH, L.N. (1998): State of molybdenum in aluminosilicate glasses. *Exp. in Geosciences* **7**, 14-16.
- ERICKSON, B.E. & HELZ, G.R. (2000): Molybdenum(VI) speciation in sulfidic waters; stability and lability of thiomolybdates. *Geochim. Cosmochim. Acta* **64**, 1149-1158.
- EVANS, J. & MOSSELMANS, J.F.W. (1991): Study of the XANES modeling of molybdenum compounds. *J. Am. Chem. Soc.* **113**, 3737-3742.
- FARGES, F. (1995) *Structures locales autour d'éléments fortement chargés dans des silicates amorphes*. HdR Dissertation, Université de Marne-la-Vallée, France.
- FARGES, F. & BROWN, G.E., JR. (1997): Coordination chemistry of Ti(IV) in silicate glasses and melts. IV. Natural and synthetic volcanic glasses. *Geochim. Cosmochim. Acta* **61**, 1863-1870.
- FARGES, F., BROWN, G.E., JR., MUNOZ, M. & PETIT, P.-E. (2001): Transition elements in water-bearing silicate glasses/melts. I. A high resolution and anharmonic analysis of Ni coordination environments in crystals, glasses, and melts. *Geochim. Cosmochim. Acta* **65**, 1665-1678.
- FARGES, F., BROWN, G.E., JR., NAVROTSKY, A., GAN, H. & REHR, J.J. (1996): Coordination chemistry of Ti(IV) in silicate glasses and melts. III. Glasses and melts between 293 and 1650 K. *Geochim. Cosmochim. Acta* **60**, 3055-3065.
- FARGES, F., BROWN, G.E., JR. & REHR, J.J. (1997): Ti K-edge XANES studies of Ti-coordination and disorder in oxide compounds: comparison between theory and experiment. *Phys. Rev. B* **56**, 1809-1819.
- FARGES, F., PONADER, C.W. & BROWN, G.E., JR. (1990): EXAFS study of the structural environments of trace levels of Zr(IV), Mo(VI) and U(VI)/U(V)/U(IV) in silicate glass/melts systems. *Trans. Am. Geophys. Union (Eos)* **70**, 1652 (abstr.).
- FARGES, F., PONADER, C.W. & BROWN, G.E., JR. (1991): Local environment around incompatible elements in silicate glass/melt systems. I. Zr at trace levels. *Geochim. Cosmochim. Acta* **55**, 1563-1574.
- FARGES, F., PONADER, C.W., CALAS, G. & BROWN, G.E., JR. (1992): Local environment around incompatible elements in silicate glass/melt systems. II. U(VI), U(V) and U(IV). *Geochim. Cosmochim. Acta* **56**, 4205-4220.
- FARGES, F. & ROSSANO, S. (2000): Water in Zr-bearing synthetic and natural glasses. *Eur. J. Mineral.* **12**, 1093-110.
- FARGES, F., SIEWERT, R., PONADER, C.W., BROWN, G.E., JR., PICHAVANT, M. & BEHRENS, H. (2006): Structural environments of incompatible elements in silicate glass/melt systems. II. Effect of temperature, pressure, H₂O, halogens, and sulfur. *Can. Mineral.* **44**, 755-773.
- FAURE, G. (1998): *Environmental Geochemistry: Disposal of Radioactive Waste* (second ed.). Prentice Hall, Upper Saddle River, New Jersey (461-484).
- GUESDON, A., BOREL, M.M., LECLAIRE, A., GRANDIN, A. & RAVEAU, B. (1994): A mixed-valent molybdenum monophosphate with a "butterfly"-shaped tunnel structure Cs₆Mo₇O₉(PO₄)₇•H₂O. *J. Solid State Chem.* **111**, 315-321.
- GUESDON, A., LECLAIRE, A., BOREL, M.M., GRANDIN, A. & RAVEAU, B. (1995): A molybdenum (V) diphosphate with a tunnel structure: β-K₂Mo₂O₄P₂O₇. *J. Solid State Chem.* **114**, 481-485.
- HEDENQUIST, J.W. & LOWENSTERN, J.B. (1994): The role of magmas in the role of hydrothermal ore deposits. *Nature* **370**, 519-527.
- HELZ, G.R., MILLER, C.V., CHARNOCK, J.M., MOSSELMANS, J.F.W., PATRICK, R.A.D., GARNER, C.D. & VAUGHAN, D.J. (1996): Mechanisms of molybdenum removal from the sea and its concentration in black shales, EXAFS evidence. *Geochim. Cosmochim. Acta* **60**, 3631-3642.
- HENDERSON, C.M.B., CRESSEY, G. & REDFERN, S.A.T. (1995): Geological applications of synchrotron radiation. *Rad. Phys. Chem.* **45**, 459-481.
- HESS, P.C. (1991): The role of high field strength cations in silicate melts. In *Physical Chemistry of Magmas* (L.L. Perchuk & I. Kushiro, eds.). Springer-Verlag, New York, N.Y. (152-191).
- HEUMANN, D., DRÄGER, G. & BOCHAROV, S. (1997): Angular-dependence in the K pre-edge XANES of cubic crystals: the separation of the empty metal eg and t_{2g} states of NiO and FeO. *J. Phys. IV Fr.* **7 C2**, 481-483.
- HILLGREN, V.J. (1993): *Partitioning Behavior of Moderately Siderophile Elements in Ni-Rich Systems: Implication for the Earth and Moon*. Ph.D. dissertation, Univ. of Arizona, Tucson, Arizona.
- HILLGREN, V.J., DRAKE, M.J. & RUBIE, D.C. (1996): High-pressure and high-temperature metal-silicate partitioning of siderophile elements: implications for core formation in the Earth. *Geochim. Cosmochim. Acta* **60**, 2257-2263.
- HOLZHEID, A., BORISOV, A. & PALME, H. (1994): The effect of oxygen fugacity and temperature on solubilities of nickel, cobalt, and molybdenum in silicate melts. *Geochim. Cosmochim. Acta* **58**, 1975-1981.
- HORNEBER, A., CAMARA, B. & LUTZE, W. (1982): Investigation on the oxidation state and the behavior of molybdenum in silicate glasses. In *Scientific Basis for Nuclear Waste Management V* (W. Lutze, ed.). Elsevier, Amsterdam, The Netherlands (279-288).

- IMAMURA, K. & HONDA, M. (1976): Distribution of tungsten and molybdenum between metal, silicate, and sulphide phases of meteorites. *Geochim. Cosmochim. Acta* **40**, 1073-1080.
- ISUK, E.E. & CARMAN, J. H. (1981): The system $\text{Na}_2\text{Si}_2\text{O}_5\text{-K}_2\text{Si}_2\text{O}_5\text{-MoS}_2\text{-H}_2\text{O}$ with implications for molybdenum transport in silicate melts. *Econ. Geol.* **76**, 2222-2235.
- ISUK, E.E. & CARMAN, J.H. (1983): Behavior of molybdenum in alkali silicate melts; effects of excess SiO_2 and CO_2 . *Lithos* **16**, 17-22.
- ISUK, E.E. & CARMAN, J.H. (1984): Transport and concentration of molybdenum in granite molybdenite systems; effects of fluorine and sulfur; discussion and reply. *Geology* **12**, 568-569.
- KEITH, J.D. & SHANKER, W.C. (1988): Chemical evolution and volatile fugacities of the Pine Grove porphyry molybdenum and ash flow tuff systems, southwestern Utah. In *Recent Advances in the Geology of Granite-Related Minerals Deposits* (R.P. Taylor & D.F. Strong, eds.). *Can. Inst. Mining Metall., Spec. Vol.* **39**, 401-423.
- KEPLER, H. & WYLLIE, P.J. (1991): Partitioning of Cu, Sn, Mo, W, U, and Th between melt and aqueous fluid in the systems haplogranite- $\text{H}_2\text{O-HCl}$ and haplogranite- $\text{H}_2\text{O-HF}$. *Contrib. Mineral. Petrol.* **109**, 139-150.
- KIHLBORG, L. (1963): Least squares refinement of the crystal structure of molybdenum trioxide. *Arkiv Kemi* **21**, 357-364.
- KRAUSE, M.O. & OLIVER, J.H. (1979): Natural widths of atomic K and L levels, K alpha X-ray lines and several KLL auger lines. *J. Phys. Chem. Ref. Data* **8**, 329-338.
- KRAVCHUK, I.F., MALININ, S.D., SENIN, V.G. & DERNOV-PEGAREV, V.F. (2000): Molybdenum partition between melts of natural and synthetic aluminosilicates and aqueous-salt fluids. *Geochem. Int.* **38**, 130-137.
- KUZMIN, A. & GRISENTI, R. (1994): Evaluation of multiple-scattering contribution in extended x-ray-absorption fine structure for MO_4 and MO_6 clusters. *Phil. Mag. B* **70**, 1161-1175.
- KUZMIN, A. & PURANS, J. (1997): X-ray absorption study of the short range order of tungsten and molybdenum ions in $\text{BaO-P}_2\text{O}_5\text{-WO}_3$ and $\text{CaO-P}_2\text{O}_5\text{-MoO}_3$ glasses. *J. Phys. IV* **7-C2**, 971-973.
- LECIEJEWICZ, A. (1965): The crystal structure of wulfenite. *Z. Kristallogr.* **121**, 158-164.
- LECLAIRE, A., BOREL, M.M., GRANDIN, A. & RAVEAU, B. (1988): A Mo(III) phosphate with a cage structure: NaMoP_2O_7 . *J. Solid State Chem.* **76**, 131-235.
- LECLAIRE, A. & RAVEAU, B. (1988): Small atomic displacements in the molybdenophosphates $\text{AMo}_2\text{P}_3\text{O}_{12}$ (A = K, Rb, Tl). *Acta Crystallogr.* **C44**, 226-229.
- LE GRAND, M. (1999): *Les platinoïdes et le molybdène dans les verres d'intérêt nucléaire. Etude structurale*. Ph.D. thesis, Univ. Paris VII, Paris, France.
- LYTLE, F.W., GREGOR, R.B., SANDSTROM, D.R., MARQUES, D.R., WONG, J., SPIRO, C.L., HUFFMAN, G.P. & HUGGINS, F.E. (1984): Measurement of soft x-ray absorption spectra with a fluorescence ion chamber detector. *Nucl. Inst. Meth.* **226**, 542-548.
- MATSUMOTO, K., KOBAYASHI, A. & SASAKI, Y. (1975): The crystal structure of sodium molybdate dihydrate, $\text{Na}_2\text{MoO}_4(\text{H}_2\text{O})_2$. *Bull. Chem. Soc. Japan* **48**, 1009-1013.
- MCMMASTER, J., CARDUCCI, M.D., YANG, Y.-S., ENEMARK, J.H. & SOLOMON, E.I. (2001): Electronic spectral studies of molybdenyl complexes. II. MCD spectroscopy of $[\text{MoOS}_4]$ centers. *Inorg. Chem.* **40**, 687-702.
- MORIN, G. & BONNIN, D. (1999): Modeling EPR powder spectra using numerical diagonalization of the full spin hamiltonian. *J. Magn. Res.* **136**, 176-199.
- MÜLLER, E., HEIDE, K. & ZANOTTO, E.D. (1992): Influence of cation coordination on nucleation in silicate glasses. *Z. Kristallogr.* **200**, 287-294.
- NYHOLM, R. & WERME, L.O. (1981): An ESCA investigation of molybdenum-containing silicate and phosphate glasses. In *Scientific basis for Nuclear Waste Management III* (J.G. Moore, ed.). Plenum Press, New York, N.Y. (101-108).
- O'KEEFE, M. & BRESE, N.E. (1992): Bond valence parameters for anion-anion bonds in solids. *Acta Crystallogr.* **B48**, 152-154.
- O'NEILL, H.St.C. & EGGINS, S.M. (2002): The effect of melt composition on trace element partitioning: an experimental investigation of the activity coefficients of FeO, NiO, CoO, MoO_2 and MoO_3 in silicate melts. *Chem. Geol.* **186**, 151-181.
- PALME, H. & RAMMENSEE, W. (1981): The cosmic abundance of molybdenum. *Earth Planet. Sci. Lett.* **55**, 356-362.
- PAULING, L. (1929): The principles determining the structure of complex ionic crystals. *J. Am. Chem. Soc.* **51**, 1010-1026.
- PETIT-MAIRE, D. (1988): *Structure locale autour d'actinides et d'éléments nucléants dans des verres borosilicatés d'intérêt nucléaire: résultats de spectroscopie d'absorption des rayons X*. Thèse de doctorat, Université Paris VI, Paris, France.
- REHR, J.J., ALBERS, R.C., NATOLI, C.R. & STERN, E.A. (1986): New high-energy approximation for x-ray-absorption near-edge structure. *Phys. Rev. B* **34**, 4350-4353.
- REHR, J. J., ALBERS, R.C. & ZABINSKI, Z.I. (1992): High order multiple scattering calculations of x-ray-absorption fine structure. *Phys. Rev. Lett.* **69**, 3397-4000.

- RIGHTER, K. & DRAKE, M.J. (1995): The effect of pressure on siderophile-element (nickel, cobalt, molybdenum, tungsten, and phosphorus) metal-silicate partition coefficients. *Meteor. Planet. Sci.* **30**, 565-566.
- RIGHTER, K. & DRAKE, M.J. (1999): Effect of water on metal-silicate partitioning of siderophile elements; a high pressure and temperature terrestrial magma ocean and core formation. *Earth Planet. Sci. Lett.* **171**, 383-399.
- ROCCA, F., KUZMIN, A., MUSTARELLI, P., TOMASI, C. & MAGISTRIS, A. (1999): XANES and EXAFS at MoK-edge in $(\text{AgI})_{(1-x)}(\text{Ag}_2\text{MoO}_4)_x$ glasses and crystals. *Sol. State Ion.* **121**, 189-192.
- RYABCHIKOV, I.D., REKHARSKY, V.I. & KUDRIN, A.V. (1981): Mobilization of molybdenum by magmatic fluids in the process of crystallization of granite melt. *Geokhimiya*, 1243-1246 (in Russ.).
- SAVARY, L., COSTENTIN, G., MAUGÉ, F., LAVALLEY, J.C., EL FALLAH, J., STUDER, F., GUESDON, A. & PONCEBLANC, H. (1997): Characterization of $\text{AgMo}_3\text{P}_2\text{O}_{14}$ catalyst active in propane mild oxidation. *J. Catal.* **169**, 287-300.
- SAWAGUCHI, N., YOKOKAWA T., & KAWAMURA, K. (1996): Mo K-edge XAFS in $\text{Na}_2\text{O}-\text{K}_2\text{O}-\text{SiO}_2$ glasses. *Phys. Chem. Glasses* **37**, 13-18.
- SCHÄFER, B., FRISCHKNECHT, R., GÜNTHER D.B. & DINGWELL, D.B. (1999): Determination of trace-element partitioning between fluid and melt using LA-ICP-MS analysis of synthetic fluid inclusions in glass. *Eur. J. Mineral.* **11**, 415-426.
- SEEDORFF, E. & EINAUDI, M.T. (2004): Henderson porphyry molybdenum system, Colorado. II. Decoupling of introduction and deposition of metals during geochemical evolution of hydrothermal fluids. *Econ. Geol.* **99**, 39-72.
- SHANNON, R.D. & PREWITT, C.T. (1969): Effective ionic radii in oxides and fluorides. *Acta Crystallogr.* **B25**, 925-946.
- SHORT, R.J., HAND, R.J., HYATT, N.C. & MÖBUS, G. (2005) Environment and oxidation state of Mo in simulated high level nuclear waste glass compositions. *J. Nucl. Mater.* **340**, 179-186.
- SIEWERT, R., FARGES, F., BEHRENS, H., BUETTNER, H. & BROWN, G.E., JR. (1997a): The effect of water on the coordination of Mo in albite glass; an high-resolution XANES spectroscopy study. *Trans. Am. Geophys. Union (Eos)* **78**(46), Suppl., 768.
- SIEWERT, R., FARGES, F., BUETTNER, H. & BROWN, G.E., JR. (1997b): Investigation of molybdenum redox state coordinations in silicate glasses and melts to 1500 K by high-resolution XANES- spectroscopy. *Ber. Deutsch. Mineral. Gesell.* **1997**, 336 (abstr.).
- SIEWERT, R., FARGES, F., BUETTNER, H. & BROWN, G.E., JR. (1998): The coordination chemistry of molybdenum in silicate glasses; a XAFS-spectroscopy study. *Terra Abstr.* **10**, 59 (abstr.).
- STEBBINS, J.F. (1995): Dynamics and structure of silicate and oxide melts: nuclear magnetic resonance studies. *In* Structure, Dynamics and Properties of Silicate Melts (J.F. Stebbins, P.F. McMillan & D.B. Dingwell, eds.). *Rev. Mineral.* **32**, 191-246.
- STEMPROK, M. (1990): Solubility of tin, tungsten and molybdenum oxides in felsic magmas. *Mineral. Deposita* **25**, 205-212.
- STEMPROK, M. & VOLDAN, J. (1974): Homogeneous silicate glass phases in systems sodium oxide – silicon oxide – tungsten trioxide and sodium oxide – silicon oxide – molybdenum trioxide. *Silikaty* **18**, 19-30 (in Russ.).
- TACKER, R.C. & CANDELA, P.A. (1987): Partitioning of molybdenum between magnetite and melt: a preliminary experimental study of partitioning of ore metals between silicic magmas and crystalline phases. *Econ. Geol.* **82**, 1827-1838.
- TEO, B.K. (1986): *EXAFS: Basic Principles and Data Analysis*. Springer-Verlag, New York, N.Y.
- TINGLE, T.N. & FENN, P.M. (1984): Transport and concentration of molybdenum in granite molybdenite systems: effect of fluorine and sulfur. *Geology* **12**, 156-158.
- TRITYAK, I.D., BILEN'KIL, B.F., MARKIV, M.V. & PANASYUK, P.V. (1974): Growth, symmetry, lattice parameters, and optical properties of lithium molybdate single crystals. *Kristallografiya* **19**, 876-877.
- WALTER, M.J. & THIBAUT, Y. (1995): Partitioning of tungsten and molybdenum between metallic liquid and silicate melt. *Science* **270**, 1186-1189.
- WEBSTER, J.D. (1999): Exsolution of magmatic volatile phases from Cl-enriched mineralizing granitic magmas and implications for ore metal transport. *Geochim. Cosmochim. Acta* **61**, 1017-1029.
- WHITE, W.H., BOOKSTROM, A.A., KAMILLI, R.J., GANSTER, M.W., SMITH, R.P., RANTA, D.E. & STEININGER, R.C. (1981): Character and origin of Climax-type molybdenum deposits. *Econ. Geol.* **75**, 270-316.
- WILKE, M., FARGES, F., PETIT, P.E., BROWN, G.E., JR. & MARTIN, F. (2001): Oxidation state and coordination of Fe in minerals: an Fe K XANES spectroscopic study. *Am. Mineral.* **65**, 713-730.
- WINTERER, M. (1997): The XAFS package. *J. Phys. IV, Colloq.* **7-C2**, 243-244.

Received November 24, 2004, revised manuscript accepted November 22, 2005.